

SPECTROSCOPIC STUDIES OF Mn/Eu DOPED PHOSPHATES, SILICATES AND BORATES

by

Teddy Alexis Rodríguez Vélez

A thesis submitted in partial fulfillment of the requirements for the degree of

MASTER OF SCIENCE
in
PHYSICS

UNIVERSITY OF PUERTO RICO
MAYAGÜEZ CAMPUS
2006

Approved by:

Dorial Castellanos, PhD
Member, Graduate Committee

Date

Pablo Marrero, PhD
Member, Graduate Committee

Date

Weiyi Jia, PhD
President, Graduate Committee

Date

Uroyoán R. Walker Ramos, PhD
Representative of Graduate Studies

Date

Héctor Jiménez, PhD
Chairperson of the Department

Date

ABSTRACT

Lighting consumes about 23% of electric energy nationwide. Any improvement in lighting efficiency will lead to huge benefits for our society. The first generation of light sources was the incandescent lamp with an energy efficiency of only 5%, and has been replaced gradually by fluorescence lamps with an energy efficiency of more than 28%. Further improvement of fluorescent lamps now encounters a bottleneck. New lighting physics concepts have been explored within the last two decades. These include quantum cutting phosphor fluorescent lamps which have become very competitive due to their high energy efficiency, low cost, small volume and weight, and long lifetime. Currently, most commercial LEDs' light sources are single color. For white LED sources, the most promising devices are phosphor-coated LEDs, in which LEDs emission is down-converted to white light. There are two kinds of designs: (a) blue LEDs plus yellow phosphors and (b) UV LEDs plus tricolor phosphors.

The purpose of this project is to search for efficient phosphors which can be used as LED-phosphors white light sources. Three groups of materials were examined: (a) phosphates, $M_2P_2O_7$ (M=Mg, Ca, Sr, Ba); (b) silicates, $A_2MSi_2O_7$ (A= Sr or Ba, and M=Mg or Zn); and borates $Ba_2MgB_2O_6$ and $LiBa_2B_5O_{10}$. These materials are single or double doped with Eu^{2+} and Mn^{2+} . All phosphors were prepared with standard ceramic technology. X-ray diffraction, photoluminescence, temperature dependence of luminescence, and the excitation spectrum of phosphors were studied. Various results were found: first, that efficient energy transfer was observed from Eu^{2+} to Mn^{2+} . This

energy transfer allows the red emission of Mn^{2+} to be enhanced by sensitization with Eu^{2+} . Secondly, in $\text{Mg}_2\text{P}_2\text{O}_7:\text{Eu}^{2+},\text{Mn}^{2+}$ and $\text{Sr}_2\text{MgSi}_2\text{O}_7:\text{Eu}^{2+},\text{Mn}^{2+}$, strong emission bands in blue and red were found under UV excitation. The phosphor then provides two basic colors. This could be an interesting application for LED-tricolor phosphor devices. Thirdly, a strong green emission was detected in $\text{Ba}_2\text{ZnSi}_2\text{O}_7$ doped with Eu^{2+} or $\text{Eu}^{2+}/\text{Mn}^{2+}$ and $\text{Ba}_3\text{ZnSi}_2\text{O}_8$ doped with Eu^{2+} or $\text{Eu}^{2+}/\text{Mn}^{2+}$. These phosphors can be used as the green component for LED-phosphor white light devices. Fourthly, $\text{Ba}_2\text{MgB}_2\text{O}_6:\text{Eu}^{2+}$ has strong orange emission near 600nm that can be used to improve color rendering in LED-phosphors devices. Finally, $\text{LiBa}_2\text{B}_5\text{O}_{10}:\text{Eu}^{2+}$ showed a blue-green emission, instead of a red emission previously reported in the literature. Although the blue-green emission may not be an ideal green component for the tricolor system, this strong UV emission provides a clue indicating that the host might be a good wide band gap semiconductor.

In addition, the energy level assignments for Mn^{2+} and Eu^{2+} , energy transfer between Eu and Mn, and the blue-shift of Eu emission bands are discussed. A modified single coordinate configuration for Eu^{2+} is proposed to explain the blue-shift of Eu^{2+} crystalline hosts.

RESUMEN

La iluminación consume 23% de la energía nacional, por lo tanto cualquier mejora en la eficiencia de las técnicas de iluminación sería de gran beneficio a nuestra sociedad. La primera generación de fuentes de luz lo fueron las bombillas incandescentes con una eficiencia de energía de solo 5%. Éstas han sido remplazadas gradualmente por las fluorescentes con una eficiencia de 28%. Muchos conceptos físicos referentes a iluminación han sido estudiados en las últimas dos décadas. Entre ellos están las bombillas de fósforos de corte cuántico, las cuales se han vuelto comercialmente muy competitivas debido a su alta eficiencia, bajo costo, pequeño peso y tamaño y larga duración. Actualmente, la mayoría de las fuentes de luz LEDs, disponibles comercialmente, tienen un solo color. En el caso de fuentes de luz LED blanca, los dispositivos más prometedores son los LEDs cubiertos de fósforos, en el cual la emisión LED es convertida en luz blanca. Hay dos tipos de diseños: (a) LEDs azules con fósforos amarillos y (b) LEDs UV con fósforos tricolor.

El propósito de este proyecto es buscar fósforos de alta eficiencia que puedan ser usados como fuentes de luz blanca de fósforos-LED. Los tres grupos de materiales que se investigaron fueron: (a) fosfatos, $M_2P_2O_7$ (M=Mg, Ca, Sr, Ba); (b) silicatos, $A_2MSi_2O_7$ (A= Sr or Ba, and M=Mg or Zn); y boratos $Ba_2MgB_2O_6$ y $LiBa_2B_5O_{10}$. Estos eran dopados o co-dopados con Eu^{2+} y Mn^{2+} . Todos los fósforos fueron preparados con tecnología de cerámica estándar. Fueron estudiados los espectros de difracción de rayos-X, la fotoluminiscencia, la dependencia de la luminiscencia respecto a la temperatura y los espectros de excitación de los fósforos. Se encontraron varios resultados: primero, se

observó transferencia de energía eficiente de Eu^{2+} a Mn^{2+} . Esta transferencia de energía proveía la oportunidad de mejorar la emisión roja de Mn^{2+} a través de la sensibilización con Eu^{2+} . Segundo, que $\text{Mg}_2\text{P}_2\text{O}_7:\text{Eu}^{2+}$, Mn^{2+} y $\text{Sr}_2\text{MgSi}_2\text{O}_7:\text{Eu}^{2+}$, Mn^{2+} , tienen una emisión intensa en rojo y azul bajo excitación de rayos UV. Estos fósforos entonces proveen dos de los colores básicos. Esto es muy interesante para aplicaciones en dispositivos de fósforos-LED. En tercer lugar, emisión verde fue detectada en $\text{Ba}_2\text{ZnSi}_2\text{O}_7$ dopado con Eu^{2+} o $\text{Eu}^{2+}/\text{Mn}^{2+}$ y $\text{Ba}_3\text{ZnSi}_2\text{O}_8$ dopado con Eu^{2+} o $\text{Eu}^{2+}/\text{Mn}^{2+}$. Estos fósforos pueden ser usados como el componente verde para fuentes de luz blanca con LED-fósforos. Cuarto, $\text{Ba}_2\text{MgB}_2\text{O}_6:\text{Eu}^{2+}$ tiene una emisión en anaranjado (600nm) muy intensa y puede ser utilizado para mejorar el índice de representación de color en los dispositivos de fósforos-LED. Y por último, nuestra muestra de $\text{LiBa}_2\text{B}_5\text{O}_{10}:\text{Eu}^{2+}$ mostró emisión verde-azul, en vez de la emisión roja reportada en la literatura. Aunque la emisión verde-azul no es la idónea para el sistema tricolor, la intensa emisión UV observada provee una buena clave que indica que el material que provee las celdas cristalinas puede ser un buen semiconductor con espacio de banda ancha.

Finalmente se discute, la asignación de niveles de energía para Mn^{2+} y Eu^{2+} , la transferencia de energía entre Eu y Mn, y el desplazamiento al azul de las bandas de emisión de Eu. Se propone unas coordenadas de configuración modificadas para Eu^{2+} para explicar el desplazamiento al azul de Eu^{2+} en las celdas cristalinas.

To my loving family, my Mother Marta, my father Teddy Sr., my sister Martita, my late grandmother Myriam and my grandfather Teodoro, and to someone that helped get through the first pages of this work my dear friend: Luis Alberto (Bebo).

ACKNOWLEDGEMENTS

During the development of my graduate studies in the Mayagüez Campus of the University of Puerto Rico lots of persons collaborated professionally and personally while I was doing my research. Without their support it would be very much impossible for me to finish my work. That is why I wish to dedicate this section to recognize their support from the bottom of my heart.

I want to start expressing a sincere acknowledgement to my advisor, Dr. Weiyi Jia for giving me the opportunity to do research under his supervision. Also I want to acknowledge the group the Society of Physics Students (SPS) and all the members for their support, specially to Yaireska Collado, Carlos Font, Freddie Santiago, Evelyn Rivera, Alexandra Santos, Giselle Miranda and Yaítza Luna. Also very important to the entire group of TeatRUM, without them my graduate life would have been very boring. I also want to thank my undergraduate assistant Legna. I also want to thank the support of my graduate committee, Dr. Marrero and Dr. Castellanos for their counseling. And also very specially, to the secretaries of the department for all their very valuable help: Lilly and Vanessa.

The Grant from NASA under grant MURC-NCCW-0088, DOE under grant DE-FG02-94ER75764, and under DOD grant DAAH04-96-10416 supported most part of my research.

Table of Contents

ABSTRACT.....	II
RESUMEN	IV
ACKNOWLEDGEMENTS.....	VII
TABLE OF CONTENTS	VIII
TABLE LIST.....	X
FIGURE LIST	XI
1 INTRODUCTION.....	2
1.1 DEVELOPMENT OF LIGHTING TECHNOLOGY	2
1.1.1 Incandescent Lamps	2
1.1.1.1 Halogen Lamps	3
1.1.2 Fluorescent Lamps	3
1.1.3 Small Frame Fluorescent Lamps	4
1.1.4 Light-Emitting Diode (LED) Lamps	5
1.2 THE BASIC PHYSICAL IDEA FOR DEVELOPING PHOSPHORS USED FOR LED	7
1.3 SUMMARY OF FOLLOWING CHAPTERS	9
2 THEORETICAL BACKGROUND	10
2.1 CONCEPT OF COLOR RENDERING	10
2.2 LED EMISSION THEORY	11
2.3 RARE EARTHS ENERGY LEVELS AND TRANSITIONS.....	13
2.3.1 Electronic Transitions	14
2.3.2 Stark Splitting	16
2.3.3 Multi-phonon Process.....	16
2.3.4 Crystal Field Splitting	17
2.4 ENERGY TRANSFER	18
2.5 SINGLE CONFIGURATION COORDINATE	21
3 EXPERIMENTAL TECHNIQUES.....	25
3.1 SAMPLE PREPARATION	25
3.2 X-RAY DIFFRACTION.....	25
3.3 PHOTOLUMINESCENCE AND EXCITATION	26
3.4 PHOTOLUMINESCENCE MEASUREMENTS AT LOW-TEMPERATURE	30
4 SAMPLE PREPARATION.....	32
5 SPECTROSCOPY OF PHOSPHATES	34

5.1	SAMPLE PREPARATION DETAILS	34
5.2	X-RAY DIFFRACTION.....	34
5.3	EXCITATION AND LUMINESCENCE SPECTRA	36
5.3.1	<i>Mg₂P₂O₇</i>	36
5.3.2	<i>Ca₂P₂O₇: 0.02Eu, 0.04Mn</i>	38
5.3.3	<i>Sr₂P₂O₇: 0.02Eu, 0.04Mn</i>	40
5.4	DISCUSSION: MN ²⁺ ELECTRONIC CONFIGURATION	41
5.4.1	<i>Electronic Configuration</i>	41
5.4.2	<i>Assignment of Energy Levels of Excitation Spectrum of Mn²⁺</i>	42
5.4.3	<i>Selection Rule</i>	43
5.4.4	<i>Energy Transfer and Sensitization</i>	43
5.4.5	<i>Evaluation of the Phosphate Phosphors</i>	44
6	SPECTROSCOPY OF SILICATES.....	46
6.1	SAMPLE PREPARATION DETAILS	46
6.2	EXCITATION AND LUMINESCENCE SPECTRA	46
6.2.1	<i>Sr₂MgSi₂O₇: 4%Eu²⁺, 8% Mn²⁺</i>	46
6.2.2	<i>Ba₂MgSi₂O₇: 4%Eu²⁺, 8% Mn²⁺</i>	48
6.2.3	<i>Ba₂ZnSi₂O₇: 4%Eu²⁺, 8% Mn²⁺ ; Ba₂ZnSi₂O₇:Eu²⁺</i>	49
6.2.4	<i>Ba₃ZnSi₂O₈:Eu²⁺, Mn²⁺ ; Eu²⁺/Mn²⁺</i>	51
6.3	LOW-TEMPERATURE LUMINESCENCE SPECTRA	56
6.3.1	<i>Sr₂MgSi₂O₇: 4%Eu²⁺, 8% Mn²⁺</i>	56
6.3.2	<i>Ba₂ZnSi₂O₇:Eu²⁺</i>	57
6.3.3	<i>Ba₃ZnSi₂O₈:Eu²⁺</i>	58
6.4	DISCUSSION.....	58
6.4.1	<i>Energy Levels of Eu²⁺</i>	58
6.4.2	<i>Eu²⁺ Energy Structure in the Crystal Lattice</i>	59
6.4.3	<i>Evaluation of the Silicate Phosphors</i>	60
7	SPECTROSCOPY OF BORATES.....	61
7.1	SAMPLE PREPARATION DETAILS	61
7.2	EXCITATION AND LUMINESCENCE SPECTRA OF LiBa ₂ B ₅ O ₁₀ :Eu ²⁺	62
7.3	EXCITATION AND LUMINESCENCE SPECTRA OF Ba ₂ MgB ₂ O ₆ :Eu ²⁺	66
7.4	LOW-TEMPERATURE LUMINESCENCE SPECTRA	68
7.4.1	<i>LiBa₂B₅O₁₀:Eu²⁺</i>	68
7.4.2	<i>Undoped LiBa₂B₅O₁₀</i>	70
7.4.3	<i>Ba₂MgB₂O₆:Eu²⁺</i>	72
7.5	DISCUSSION: BLUE-SHIFT OF EMISSION BANDS	73
8	CONCLUSIONS AND FUTURE WORK	77
9	REFERENCES	78
APPENDIX A	TABLE OF THE SAMPLES PREPARED.....	81

Table List

Tables	Page
Table 1 Previously studied Phosphors for fluorescent lamps (LCG)	8
Table 2 Results for the Phosphates	45
Table 3 Results for the Silicates.....	60
Table 4 Results for the Borates.....	64
Table 5 Results for all the samples prepared during this research.....	82

Figure List

Figures	Page
Figure 1 Schematic of a LED.....	12
Figure 2 A schematic illustration of a configurational coordinate model	23
Figure 3 Schematic of the Fluoromax 2 System.....	27
Figure 4 Schematic of the Firing-sample preparation.....	32
Figure 5 XRD Pattern for $Mg_2P_2O_7$	35
Figure 6 XRD Pattern for $Ca_2P_2O_7$	35
Figure 7 XRD Pattern for $Sr_2P_2O_7$	36
Figure 8 Luminescence and Excitation Spectrum of $Mg_2P_2O_7:0.02Mn$	37
Figure 9 Luminescence and Excitation Spectrum of $Mg_2P_2O_7:0.02Eu, 0.04Mn$	38
Figure 10 Luminescence and Excitation Spectrum of $Ca_2P_2O_7:0.02Eu, 0.04Mn$	39
Figure 11 Luminescence and Excitation Spectrum of $Sr_2P_2O_7:0.02Eu, 0.04Mn$	40
Figure 12 Sugano-Tanabe diagram.....	42
Figure 13 Luminescence and Excitation Spectra of $Sr_2MgSi_2P_2O_7:4\%Eu^{2+}, 8\%Mn^{2+}$	47
Figure 14 Luminescence and Excitation Spectrum of $Ba_2MgSi_2O_7:4\%Eu^{2+}, 8\%Mn^{2+}$	49
Figure 15 Luminescence and Excitation Spectrum of $Ba_2ZnSi_2O_7:Eu^{2+}, Mn^{2+}$	50
Figure 16 Luminescence and Excitation Spectrum of $Ba_2ZnSi_2O_7:Eu^{2+}$	51
Figure 17 Luminescence and Excitation Spectrum of $Ba_3ZnSi_2O_8:Mn^{2+}$	53
Figure 18 Luminescence and Excitation Spectrum of $Ba_3ZnSi_2O_8:Eu^{2+}$	54
Figure 19 Luminescence and Excitation Spectrum of $Ba_3ZnSi_2O_8:4\%Eu^{2+}, 8\%Mn^{2+}$	55
Figure 20 Low-temperature Luminescence Spectra of $Sr_2MgSi_2O_7:4\%Eu^{2+}, 8\%Mn^{2+}$	56
Figure 21 Low-temperature Luminescence Spectra of $Ba_2ZnSi_2O_7:Eu^{2+}$	57
Figure 22 Low-temperature Luminescence Spectra of $Ba_3ZnSi_2O_8:Eu^{2+}$	58
Figure 23 XRD Pattern for $LiBa_2B_5O_{10}:Eu^{2+}$	63
Figure 24 XRD Pattern for $LiBa_2B_5O_{10}$	63
Figure 25 Luminescence and Excitation Spectrum of $LiBa_2B_5O_{10}:Eu^{2+}$	64
Figure 26 Drawing of the structure of $LiBa_2B_5O_{10}$	65
Figure 27 XRD Pattern for $Ba_2MgB_2O_6:Eu^{2+}$	67
Figure 28 Luminescence and Excitation Spectrum of $Ba_2MgB_2O_6:Eu^{2+}$	68
Figure 29 Low-temperature Luminescence Spectra of $LiBa_2B_5O_{10}:Eu^{2+}$	69
Figure 30 Low-temperature Luminescence Spectra of $LiBa_2B_5O_{10}:Eu^{2+}$	69
Figure 31 High-resolution Luminescence Spectrum of $LiBa_2B_5O_{10}:Eu^{2+}$	70
Figure 32 High-resolution Luminescence Spectrum of $LiBa_2B_5O_{10}$	71
Figure 33 Low-temperature Luminescence Spectra of $Ba_2MgB_2O_6:Eu^{2+}$	72
Figure 34 SCC Model for $3d$ Ions.....	73
Figure 35 Schematic of the Blue-shift theory Energy Levels.....	75

1 INTRODUCTION

1.1 Development of Lighting Technology

The improvement of light sources, including their volume, weight, lifetime decreasing power consumption has been an on-going issue since man discovered fire and invented the first lighting device. At the present time, light sources consume from 20 to 23% of electric energy nation-wide. Therefore, the improvement of energy efficiency of light sources continues to be an important issue. The energy efficiency of conventional incandescent lamps is only about 5%. For fluorescent lamps, the efficiency has reached almost 30%. Great efforts have been made to further improve the energy efficiency of these lamps, but not significant improvement has been made in decades. On the other hand, the efficiency of Light-Emitting Diodes (LEDs) continuously increases and has become very competitive. Some LED devices with single colors (red, yellow and green) have been used for traffic lights, especially in big cities. However, is difficult to make white light sources from LEDs devices, for the purpose of general illumination.

A brief introduction, a description of all relevant lighting techniques follows.

1.1.1 Incandescent Lamps

Incandescent lighting uses filament, through which electrons run and produce light through electrical resistance and the heating process. This complete process is called incandescence or thermal radiation. The bulb is kept in either a vacuum or low-pressure noble gas environment in a glass capsule. The filament most widely used is tungsten (W) due

to its relatively long life, and its resistance to high temperatures, which is important since the filament is usually heated up to around 3000 K. The problem with this type of lighting is the evaporation of the filament which makes the lifetime of these devices relatively short compared with other lighting techniques.

1.1.1.1 Halogen Lamps

Another type of incandescent lamp is the halogen lamp, originally invented to address the filament-evaporation issue by putting a halogen gas to chemically redeposit the evaporated filament. Even though this improves the lifetime and brightness of the bulbs it adds other side effects. For example, since temperatures are higher and ordinary glass is not feasible, quartz glass is used instead. Perhaps the most significant side effect of using quartz glass is that the bulb emits UV light, because quartz is transparent to this spectral range. In other words, it is possible to get a “sunburn” from excess exposure to the light of a quartz halogen bulb. As a result these devices are usually armed with a protective UV-filter. These devices are usually found in a car’s headlights and in some other domestic applications (devices).

1.1.2 Fluorescent Lamps

Fluorescent lamps use electricity to excite mercury vapor in either argon or neon gas, and this produces short-wave UV light. This light then causes the phosphor to fluoresce, or in other words produce visible light. The schematic is quite simple: the inner coat of the bulb has phosphor salts, then the bulb’s cathode emits electrons which initiate the plasma causing it to bombard electrons to the mercury vapor and therefore the vapor emits UV light, which is

absorbed by the coating and any UV emission is blocked by the bulb's glass. Fluorescent lamps are more efficient than incandescent lamps and they also out-live incandescent lamp. Unfortunately, this technology focused on in improving energy efficiency and the lower cost of production, but the final product produced lighting with a purplish or greenish hue (low color rendering index) and some magnetic ballast cycled in a frequency perceptible by the human eye, which can cause some people to become nauseous and susceptible to some types of brain seizures.

1.1.3 Small Frame Fluorescent Lamps

The first generation of fluorescent lamps has a quite large volume. Therefore, they are used mostly in industry and offices, but seldom used in resident houses. The small frame fluorescent lamps or compact fluorescent (CF) lamps function similar to fluorescent lamps, but are more suitable for residential use. The difference of these two is that CF has a tri-color phosphor in the inner coat instead of a single phosphor, and this tri-phosphor coating allows the bulb to be smaller. The issue of the fluorescent lamp was the Color Rendering Index (CRI), a concept that will be discussed later, which is greatly improved by the CFs with an index of 87 of 100, which is outstanding for a fluorescent lamp. Incandescent bulbs have an index 97, because they have a full spectrum present in the light that they emit. These bulbs are also affected by room temperature: very cool temperature causes mercury vapor to condense and condensed atoms are not be able to emit UV. On the other hand, high temperature causes too much mercury vapor and this causes some UV to be absorbed before

it excites the tri-phosphors. In either case the light output is decreased. The best temperature for these devices is between 0 °C - 38 °C.

1.1.4 Light-Emitting Diode (LED) Lamps

LED lamps were first available in single color, being the first and most popular the red. The efficiency and brightness LED lamps have improved enormously over the last few years, in particular in the blue spectral region. Blue LEDs were not available a decade ago because the semiconductor alloy needed to achieve a blue color was not fully developed. In the last years, high efficiency in blue LEDs was achieved with a new semiconductor chemistry based on gallium nitride. This new GaN alloy now allows a very high brightness blue emission. This discovery has been tested lately to generate white LED color by harnessing the blue emission with a thin coat of phosphor over the blue emitting LED.

Currently, there are two parallel directions of developing new light sources, both of which involve in research of new phosphors. One is so-called quantum cutting or quantum splitting. Quantum splitting phosphors (QSP) are those which, on average, produce more than one visible photon for each incident ultraviolet photon. Lately, most universities and commercial industries are focusing at this effect to improve different types of fluorescent lighting and reduce pollution and the economical cost of mercury. This technique uses multi-photon phosphors to cut UV photons into several visible photons and to improve the quantum efficiency up to 200% or 300%. Therefore energy efficiency can be greatly improved. The second regime combines LEDs and phosphors, and the devices are called LED-phosphor light sources. In these devices, short wavelength emission of LEDs is used to pump

phosphors and produce white light. Currently, the best devices are a combination of GaInN LED (emission at 460nm) and a phosphor $\text{Y}_3\text{Al}_5\text{O}_{12}:\text{Ce}^{3+}$ (emission band at 540nm). At the present stage, the luminance reached 50 lum/watt (compared with 80 lum/w of fluorescent lamps) with color rendering index of 85.

As one can notice the need of developing stable white light sources with the LED-phosphor approach is in an all-time high. There are two types of LED-phosphor devices in developing: first, blue LED combined with yellow-red phosphors, and second, UV LEDs combined with tri-color phosphors (460nm, 520nm and 620nm). In the first combination, InGaN chips are used to produce blue emission at 460nm. A yellow YAG:Ce phosphor, with emission-band near 540nm is coated onto InGaN LEDs. The combination of part of the blue emission of the LEDs and the yellow emission of the phosphor will produce white color. This type of devices has been intensively studied and already commercialized. However, the color rendering needs to be further improved, because of lacking of red component. The second type of devices have been studied, to less extent, and more work needs to be done on the development of tri-color phosphors.

In this project, we widely searched for new phosphors which have higher energy efficiency and have emission bands either in red or in the tricolor wavelengths defined above. These phosphors can be used to improve energy efficiency and color rendering of LED-phosphor white light sources. In previous years, red phosphor of Pr doped CaTiO_3 has been successfully studied and UV excitation efficiency has been greatly improved in our lab (Rivera-Figueroa 2001). We investigated Eu^{2+} and Mn^{2+} doped and co-doped silicates, such as $\text{Sr}_2\text{MgSi}_2\text{O}_7$; borates, such as $\text{MgBa}_2\text{B}_2\text{O}_6:\text{Eu}^{2+}$, and phosphates $\text{M}_2\text{P}_2\text{O}_7$ (M=Mg, Ca, Sr,

Ba). Solid chemical reaction method was used to prepare the samples. X-ray diffraction pattern, emission and excitation spectra were measured. Temperature dependence of luminescence was investigated. The result and possibility in application to LED-phosphors devices will be discussed.

1.2 The Basic Physical Idea for Developing Phosphors used for LEDs

Phosphors used for fluorescent lamps have been intensively studied. Many kinds of emission ions are used in these materials. Including Mn^{2+} , Mn^{4+} , Cu^+ , Sn^{2+} , Pb^{2+} , Tl^{3+} , Bi^{3+} , and various rare earth ions, such as, Ce^{3+} , Pr^{3+} , Eu^{3+} , Eu^{2+} and Tb^{3+} . Among these ions, we are especially interested in Mn^{2+} and Eu^{2+} . Table 1 lists the emission wavelength of some phosphors doped with these two ions.

Mn^{2+} has been known to produce green to red luminescence in lots of inorganic compounds, depending on the crystal field strength of the substituted sites. In tetrahedron sites, Mn^{2+} usually emits at green, while in octahedron sites, it emits in orange or red. In fact, due to the possibility to tailor the emission wavelength, many Mn^{2+} doped phosphors were developed and are used widely for fluorescent lamps. Some of the studied materials and their peak wavelengths are listed in Table 1. However, electronic transitions of Mn^{2+} are spin forbidden, and the absorptions in UV or deep blue spectral range are weak. This is certainly a disadvantage for applications in our case. On the other hand, Eu^{2+} usually gives a strong and broad-band absorption and emission due to the nature of $f-d$ transitions. Eu^{2+} can change its emission wavelength from near-UV to red depending on the hosts. It has also been found

that energy transfer may occur from Eu^{2+} to Mn^{2+} in some hosts. This provides us an opportunity to use Eu^{2+} as a sensitizer for Mn^{2+} . Eu^{2+} ions absorb LED UV or deep blue emission and transfer the photo-energy to Mn^{2+} , which may emits in red (see table 1).

Luminescence Center	Chemical Composition	Peak wavelength (nm)	Luminescence Color
Eu^{2+}	$\text{SrB}_4\text{O}_7\text{F}:\text{Eu}^{2+}$	360	Ultraviolet
	$\text{SrMg}_2\text{O}_7:\text{Eu}^{2+}$	394	Blue
	$(\text{Sr},\text{Ba})\text{Al}_2\text{Si}_2\text{O}_8:\text{Eu}^{2+}$	400	Blue
	$\text{Sr}_3(\text{PO}_4)_2:\text{Eu}^{2+}$	408	Blue
	$\text{Sr}_2\text{P}_2\text{O}_7:\text{Eu}^{2+}$	420	Blue
	$\text{Ba}_3\text{MgSi}_2\text{O}_8:\text{Eu}^{2+}$	435	Blue
	$\text{Sr}_{10}(\text{PO}_4)_6\text{Cl}_2:\text{Eu}^{2+}$	447	Blue
	$\text{BaMg}_2\text{Al}_{16}\text{O}_{27}:\text{Eu}^{2+}$, Mn^{2+}	450, (515)	Blue
	$(\text{Sr},\text{Ca})_{10}(\text{PO}_4)_6\text{Cl}_2:\text{Eu}^{2+}$	452	Blue
	$(\text{Sr},\text{Ca})_{10}(\text{PO}_4)_6\text{nB}_2\text{O}_3:$ Eu^{2+}	452	Blue
	$\text{BaMg}_2\text{Al}_{16}\text{O}_{27}:\text{Eu}^{2+}$	452	Blue
	$\text{Sr}_2\text{Si}_3\text{O}_8 \cdot 2\text{SrCl}_2:\text{Eu}^{2+}$	490	Blue-Green
	$\text{Sr}_3\text{Al}_2\text{O}_4:\text{Eu}^{2+}$	520	Green
	Mn^{2+}	$\text{MgGa}_2\text{O}_4:\text{Mn}^{2+}$	510
$\text{BaMg}_2\text{Al}_{16}\text{O}_{27}:\text{Mn}^{2+}$		(450), 515	Green
$\text{ZnSiO}_4:\text{Mn}^{2+}$		525	Green
$\text{GdMgB}_5\text{PO}_{10}:\text{Ce}^{3+}, \text{Tb}^{3+}$, Mn^{2+}		543, 630 (480), 575	Yellow Warm white
$3\text{Ca}_3(\text{PO}_4)_2\text{Ca}(\text{F},\text{Cl})_2:$ $\text{Sb}^{3+}, \text{Mn}^{2+}$			
$\text{CaSiO}_3:\text{Pb}^{2+}, \text{Mn}^{2+}$		610	Orange
$\text{Cd}_2\text{B}_2\text{O}_5:\text{Mn}^{2+}$		620	Pink
$\text{GdMgB}_5\text{O}_{10}:\text{Ce}^{3+}, \text{Mn}^{2+}$		630	Orange
$\text{GdMgB}_5\text{O}_{10}:\text{Ce}^{3+}, \text{Tb}^{3+}$, Mn^{2+}		(543), 630	Orange

Table 1 Previously studied Phosphors for fluorescent lamps (LCG) (Shionoya and Yem 1999)

1.3 Summary of Following Chapters

Chapter 2 introduces theoretical background of luminescence of $3d$ ions and rare-earths. Experiments and instrumentation are described in Chapter 3. Details of the sample preparation and materials used are presented in Chapter 4. Chapters 5, 6 and 7 present the results of phosphates phosphors, silicate phosphors and borate phosphors, respectively, and discuss some experimental results including assignment of energy levels of emission and excitation spectra, energy transfer between Eu^{2+} and Mn^{2+} and blue-shift of Eu^{2+} emission bands with increasing temperature. Conclusions are presented in Chapter 8.

2 THEORETICAL BACKGROUND

2.1 Concept of Color Rendering

The Color Rendering Index (CRI) is a very important concept in the lighting industry; this number describes how accurate the color of the objects will appear under a specific light source. This number varies in a range of 0-100, 100 being the perfect CRI. This index is independent of the color temperature which describes how the light appears when the human eye looks directly at an illuminated bulb, and this color temperature parameter is obviously dependent on the temperature of the bulb. Different lighting techniques have different CRIs, usually the best CRIs (95⁺) are usually found in the incandescent lamps. A good CRI is considered to be in the range of 85-90 and an excellent one is from 90 and up. This index is very important because it will tell you how accurate the color discrimination will be under this light source. For example a light source like a low-pressure sodium vapor lamp, which actually monochromatic, the CRI is nearly zero. In the contrary, for a source like an incandescent light bulb, the CRI is near a hundred.

CRI is determined by comparing the color shifts of objects when they are illuminated by the light source and by a reference light source which has a comparable color temperature. A palette of fifteen colors is used to measure the color the ration of normalized light intensity of the light source against the reference light. This test is called the General Color Rendering Index, and the calculations are just the difference of each color sample illuminated by the

reference and the light source under test. Later the results for each sample are averaged and scored in a scale from 0 -100, which we previously discussed.

2.2 LED Emission Theory

LED emits light from electronic transitions in a layered semiconductor. It consists of an alloy crystal placed in a reflective cup which is chemically bonded to wires, and then this circuit is encapsulated in epoxy. Then when electric current runs through the wires, the material is excited. This excitement is translated in energy, a small part of which converts into heat, but most of it converts to light. The color of the light obviously depends on the alloy crystal. LEDs have a *p*-type and *n*-type semiconductor connected and this is called a *p-n* junction or a diode. A *p*-type semiconductor has the valence band partially empty and has an empty conduction band; in the other hand the *n*-type semiconductor has the valence band full and the conduction band partially filled. When current flows through the circuit the electrons will occupy the conduction band of the *n*-type, later the electrons will be pushed to the *p*-type side of the junction and then they will go to the conduction band of the *p*-type semiconductor. And since they already occupy the higher-energy band in the *n*-type side, even though electrons that are in the higher energy band of the *p*-type semiconductor, will fall into the lower energy band if there is available space in the valence band, the electrons that fall from the higher energy band (the conduction band) to the lower energy band in the

p-type side will be more stable. Then the electrons that cross the band gap will cause energy release, related to the size of the gap, in form of light.

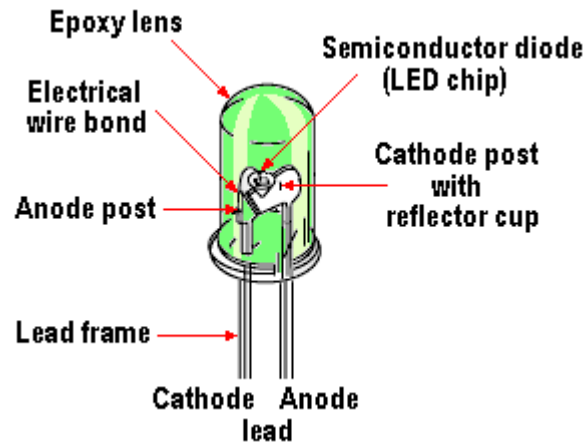


Figure 1 Schematic of a LED

When light from all the wavelengths of the visible spectrum are present, this mixture of colors appears white. However, the human eye does not require this mixture of all the colors to perceive white light. Primary colors from the upper (red), middle (green), and lower (blue) parts of the spectrum, when combined, will appear white. To achieve this tri-color combination with LEDs requires very sophisticated electro-optical designs to control the diffusion and the mixture of colors.

To produce white light sources, we may need tricolor phosphors to meet the following requirements:

- a. Phosphors with emissions of three primary colors: blue near 450nm, green near 520nm and red near 620nm, respectively.

- b. To ensure the color quality, the width of the emission bands should be greater than 50nm.
- c. Have strong absorption in the spectral range of 380-400nm (herein called UV C-band or the C-band) or 460nm.
- d. High stability and low degradation.

2.3 Rare Earths Energy Levels and Transitions

There are fourteen rare earth elements and they lie between lanthanum (^{57}La) and hafnium (^{72}Hf). Their atomic configurations consist of partially filled $4f$ shells. It is important to note that ions with either filled $4f$ levels such as Lu^{3+} or ions that have no $4f$ electrons such as La^{3+} , will have no electronic energy levels to induce excitation in/or near the visible region.

The azimuthal quantum number (ℓ) of $4f$ orbitals is 3, which gives $2\ell + 1 = 7$ orbital state (7 orbital orientation) and allows 14 electrons to stay. In the non-excited state this electrons will be distributed in such a way that it will have the maximum combined spin angular momentum (S). According to Hund's rule the spin angular momentum S is added to the orbital angular momentum L to give the total angular momentum J. For the lowest ground state, $J=L-S$, when the number of $4f$ electrons is less or equal to 7, and $J=L+S$, when the number of $4f$ electrons is larger than 7.

2.3.1 *Electronic Transitions*

An electronic state is indicated by notation $^{2S+1}L_J$, where L represents the letters S, P, D, F, G, H, I, K, L, M, N... corresponding to the resultant orbital quantum number of $4f$ electrons $L=0, 1, 2, 3, 4, 5, 6, 7, 8...$ respectively (Henderson and Imbusch 1989). An electronic state is actually expressed as an intermediate coupling state and can be described as a mixed state of several $^{2S+1}L_J$ states and a spin-orbit interaction. This mixing due to spin-orbit is actually small for the levels near the ground states, and it is larger for the states that are neighbors with the same J numbers. The effect of the mixing is very large in the optical transition probabilities, though is relatively small on the energy levels. Rare earth ions (doubly or triply charged) can be present in ionic solids. For the case of the triply charged, all $5d$ and $6s$ orbitals are empty and the $4f$ is partially occupied. The optically active $4f$ electrons are shielded from the crystalline electric field by the outer $5s$ and $5p$ shells. The resulting effect is that the neighboring ligands have very little affection on the $4f$ electrons. The energy levels of the $4f$ electrons are very similar to the free ion levels characterized by the L, S and J values with allowance made for some term mixing (Henderson and Imbusch 1989) and this is because of the weak interaction with the lattice environment. The spectral lines (either of emission or absorption) are sharp and the energy positions are not (usually) crystalline host dependent.

For the case of divalent rare-earth ions, the energy separation between the $4f^n$ and $4f^{n-1}5d$ configurations will be large and the transitions between these two may be observed by normal spectroscopy. These transitions are dipole-allowed and are about 10^6 times stronger

than the very frequently observed $4f \rightarrow 4f$ transitions in trivalent (rare-earth) ions. The emission and excitation spectra of the divalent europium ion are mainly composed of two types of electronic transitions: a strong $4f \rightarrow 5d$ transition with a high energy and a weak $4f \rightarrow 4f$ transition at low energies. The gross feature of the spectra of this type of rare-earth ions is considered to arise from the T_{2g} and E_g components of the $5d$ electron in the cubic crystalline field. The strongest lines were actually assigned to pure electronic transitions from $4f^n$ to $4f^{n-1}5d$ which was assumed to be caused by the interaction between the $4f^{n-1}$ core and the $5d$ electron, the $4f^{n-1}5d$ level being spaced with the energy gaps in the $4f^{n-1}$ ground multiplets (Rubio O. 1991).

Optical absorption of $4f$ electrons transitions are strongly forbidden by the parity selection rule (Blasse and Grabmaier 1994). However, this rule can be relaxed. When an ion occupies a crystalline site there are uneven components of the crystal-field. These components mix a small amount of opposite parity wavefunctions into the $4f$ wavefunctions, and this causes intra-configurational $4f$ transitions to gain some intensity.

The allowed optical inter-configurational transitions for rare earth ions are divided in two types: $4f^n \rightarrow 4f^{n+1}L^{-1}$, L=ligand (charge-transfer transitions) and $4f^n \rightarrow 4f^{n-1}5d$ transitions. And both are allowed and have broad absorption band. The first type of charge transfer is found in rare earth elements that like to be reduced and is commonly observed in tetravalent rare earth ions. The second ($5d$ transition) in the other hand is found for the ones which like to be oxidized and is commonly observed in divalent rare earth ions.

2.3.2 *Stark Splitting*

As mentioned before $4f$ electrons of rare earth are shielded from crystal environment by $5s$ and $5p$ shells. However, in a crystal field, the J degeneracy of spin-orbit state $^{2S+1}L_J$ can be shifted and split. This is called Stark splitting. In other words this effect is the splitting of the spectral line into several components in the presence of an electric field. This effect is the analogous to the Zeeman effect in a magnetic field, but in this case the splitting is not symmetric. This splitting only occurs when the ion is polarized by the electric field resulting in a dipole moment. This dipole moment only depends upon magnitude (M_j), not direction, so the energy levels will be split into $J+1$ or $J+1/2$ levels.

This splitting is usually much less than the separation of the spin-orbit levels. Because of this, the main features of the energy levels diagrams remain almost unchanged for the rare earth ions in different host materials. In the other hand, the crystal field splitting will vary for different host, and it will show the different symmetries and strengths of the crystal fields.

2.3.3 *Multi-phonon Process*

Most $4f$ emitting levels are separated from the next lower level in a distance of at least $2 \times 10^3 \text{ cm}^{-1}$. Excited states of this kind release their energy via either of two competitive ways: light emission or by phonon emission. The rate of phonon emission is dependent on the number of phonons emitted at the same time to bridge the energy gap. The probability of multiple phonon transitions is given by the relation:

$$w \propto \exp\left(-k\Delta E/h\nu_{\max}\right),$$

where w is the phonon transition rate, ΔE is the energy gap closest to the lower level and $h\nu_{max}$ is the maximum energy of phonons (coupled to the emitting states). When ΔE increases the phonon emission rate decreases rapidly, therefore the competitive light emission process (radiative) becomes the dominant one. In the contrary, if the phonon energy is large or ΔE is small, the phonon transition probability can be very high, and the radiative transition of the upper excited level can be seriously quenched.

2.3.4 *Crystal Field Splitting*

Wavefunctions of $5d$ of rare earth such as Eu^{2+} and $3d$ electrons of transition ions such as Mn^{2+} are quite extended. They will strongly interact with ligand ions in crystals. As a result, the resultant orbital states of d electrons will be split. The splitting is usually much larger than the splitting by L-S coupling. Crystal field splitting depends on several factors:

- (1) number of electrons in the d orbitals
- (2) oxidation state of the crystal (a high oxidation state will lead to a high energy-splitting)
- (3) the arrangement of the ligands around the crystal
- (4) the nature of the ligands

The most common type of complex is the octahedral. In this case six ligands form an octahedral field around the metal ion and the ligands point directly into the d -orbitals and cause high-energy splitting. The second most common type of complex is the tetrahedral, for this case four ligands form a tetrahedral field around the metal ion for this case the electrons are not oriented directly against the orbitals, therefore the energy splitting level is lower than

the previous case. The physics of this phenomenon is the following: as we know the transition metals have ions with partially filled orbitals (five of them) and they are degenerate. When a ligand approaches the metal ion, the electrons from the ligand are at different distances to the d -orbitals, and the electrons in the d -orbitals and the ones in the ligand have an acting repulsive force, because the d -orbitals are repulsed unequally by the ligand, and obviously the d -orbitals will split in energy.

In some cases there are more than one d -electron and in these cases we observe a strong crystal field. These electrons affect each other electro-statically through a potential of the form:

$$\sum \frac{e^2}{r}.$$

2.4 Energy Transfer

The process in which the excitation of a certain ion migrates to another ion is called energy transfer. It is very important to understand this effect in order to develop efficient luminescent materials. The luminescent materials had several types of energy transfer (Goldberg 1966):

- i. ***Resonant energy transfer between ions of same energy level*** – for this case the excitation energy of a certain ion migrates to another one of the same species that is in the ground state. This type of transfer is also divided in three categories: first, multi-polar interaction, and, this is, both transitions are of electric dipole character; the second is the exchange interaction, and

this is, when the donor and the acceptor are both located so close that their electronic wavefunctions overlap and the transfer is due to a quantum mechanical interaction; and lastly the phonon-assisted energy transfer, which occurs when there is a difference ΔE between the transition energies of the donor and the acceptor, and is compensated by either a phonon emission or absorption.

- ii. ***Spectral diffusion*** – in this case the excited ion can give its energy to other ions that are at different sites and/or lattice environment, due to the fact that the doping ions stay at a slightly different lattice environment. This will translate to a shift in the emission spectrum to longer wavelengths and an increment on the width of the emission peak.
- iii. ***Energy donation*** – in this case the energy transfer can occur between different ions, one of them is called a donor and the other an acceptor. An ion at an excited higher energy level can transfer most of its energy to other ions. The other ions stay at a lower energy levels and release the differential energy in form of phonons.
- iv. ***Sensitizer's transfer*** – a donor that usually has a strong absorption of external radiation and transfers it very efficiently to an acceptor is called a

sensitizer; the caused emission is greatly enhanced. This process is also known as sensitization of the luminescence.

- v. ***Quenching centers transfer*** – in this case the acceptor kills the emission of the active center or the donating ions, and these ions neither emits at the required wavelength nor emits at all. Most the phosphors that exhibit this type of luminescence are activated by sensitizers or co-activators (i.e. Mn^{2+}).

It is important to determine the optimum concentration of dopant to be used, in order to obtain efficient luminescence with a minimum energy loss. For display application, the purity of color is the most important issue. For many ions emissions can be from different upper excited states. The way to keep this emission from the upper states from occurring, and to purify the luminescence is to quench the emission via cross relaxation (Nakazawa & Shionoya 1970). In this process, the excited ions from the upper states prefer to release part of their energy to the neighboring ions at the ground state, and then move to the lowest meta-stable state. Then these ions will return to the ground state and release the remaining energy at the desire wavelength. In order to be able to do this, the doping concentration should be sufficiently high, but it is important to note that in a heavily-doped system the average distance between the ions becomes smaller and therefore, the excited ions can move around in the host causing resonant energy transfer. Such transfer gives more chance to send the excitation to a quenching center, which will release the energy through a non-radiative

process. This phenomenon is called concentration quenching, as we briefly described earlier. A compromise concentration should then be determined and this will give an efficient sensitization (efficient upper-state quenching) and a maximization of the number of activators to participate in the luminescence process. However, the concentration should not lead to any concentration quenching. These centers also can produce an undesired afterglow (Jia et. al 2000). The sensitization is used to enhance the energy excitation efficiency.

2.5 Single Configuration Coordinate

It is important to discuss the classical Configuration Coordinate Model, which is often used to explain optical transitions and the effects of lattice vibrations on localized centers. In this model, the luminescence ion and nearest neighbor ions site are selected for simplicity. These ions can be regarded as lonely molecules by neglecting the effects of far positioned ions. This way a small number of specific normal coordinates can be used to approximate the large number of vibrational modes of the lattice. These coordinates are called configurational coordinates. This model explains the optical properties of localized centers on the basis of potential curves, and these curves represent the total energy in its respective state as a function of the mentioned coordinate. This total energy is the sum of the lattice vibration energy and electron energy. The configurational coordinate model is built similarly to the adiabatic potential of a diatomic molecule, where the variable on the abscissa is the inter-atomic distance. In contrast, the adiabatic potential of a multiple-atom molecule requires a multi-dimensional space, but it is approximated by a single configurational

coordinate, which is one-dimensional. The symmetry of the vibrational mode is usually employed in this model. This model can be used to explain qualitatively the following:

- (a) Stoke's law; the fact that the energy of excitation is higher than the emission in most cases and that the energy difference between these two is called the Stoke's shift.
- (b) The widths of excitation or emission bands and their temperature dependence.
- (c) The thermal quenching of luminescence.

Following the path of the optical transitions showed in Figure 2, and presuming that we express the bonding force between the luminescence ion and a nearest-neighbor ion, the deviation from the equilibrium position in the ground state as the configurational coordinate is denoted as Q . The relationship between the total energy of the ground state and the excited state, which are denoted as U_g and U_e respectively, are given by:

$$U_g = K_g \frac{Q^2}{2}$$
$$U_e = K_e \frac{(Q - Q_0)^2}{2} + U_0,$$

where K_e and K_g are the force constants of the chemical bond for the excited and the ground state respectively, U_0 is the pure electronic energy at the excited state, and Q_0 is the shift distance of the equilibrium position of the excited state from the ground state equilibrium position. (Shionoya and Yen 1999)

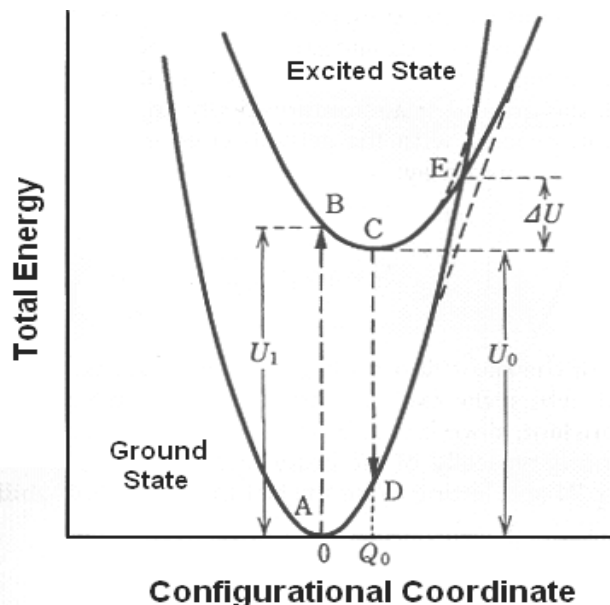


Figure 2 A schematic illustration of a configurational coordinate model. The two curves are modified by repulsion near the intersection (broken lines). The vertical broken lines $A \leftrightarrow B$ and $C \leftrightarrow D$ indicate the absorption and emission of light, respectively. (Shionoya and Yen 1999)

The spatial distribution of an electron orbital is obviously different between the ground and excited state, giving rise to a difference in the electron wave function overlap with vibration wavefunction of the neighboring ions. This difference further produces a change in the position of the equilibrium and the value of the force constant of the ground and excited state, and is the origin of the Stoke's shift. In the excited state, the orbital has a bigger radius, so that the energy of this electron orbital depends less on the configuration coordinate.

In Figure 2, optical absorption and emission process are shown by vertical broken arrows. As seen the nucleus of the emitting ion stays approximately at the same position throughout the optical processes of the electron (Frank-Codon Principle). It is reasonable to

do this approximation because the atomic nucleus is 10^3 to 10^5 time heavier than an electron. The A-B arrow shows the optical absorption proceeding from equilibrium position of the ground state at 0K. The probability of an excited electron to lose energy by generating lattice vibration is 10^{12} to 10^{13} s^{-1} , on the other hand the probability of losing the energy by light emission is at the most 10^9 s^{-1} . Therefore, state B relaxes to equilibrium position C before emitting. This process is followed by the emission $C \rightarrow D$ and the relaxation $D \rightarrow A$, closing the cycle. At finite temperature, the electron state will oscillate around the equilibrium position along the configurational coordinate curve up to the thermal energy of kT . The amplitude of this oscillation broadens the spectral width of the excitation transition.

It is also relevant to note that an excited electron can cross the intersection E assisted by thermal activation, and can reach the ground state non-radiatively when two configurational coordinates' curves intersect. That means that one can assume a non-radiative relaxation process with activation energy ΔU , and with a transition probability N per unit time given by:

$$N = s \exp\left(\frac{-\Delta U}{kT}\right),$$

where s is a product of the transition probability between the excited and the ground states and the frequency in which the excited state reached the intersection E. The value of s can be treated as a constant, since the dependence on the temperature is weakly. This is called the frequency factor and is usually in the order of 10^{13} s^{-1} .

3 EXPERIMENTAL TECHNIQUES

3.1 Sample Preparation

The samples were prepared with solid-state chemical reaction. The corresponding chemicals of each phosphor are mixed and ground in a mortar to form a uniform powder, then pressed to form a pellet under a pressure of 5,000 lb/in². The pellets then were pre-fired for two hours approximately at a raising rate of 5° C/min, and then the pellets are ground again to form a homogeneous powder. Then the pellets were finally fired in an atmosphere of H₂ + 5%N₂ gas at their sintering temperature, in order to reduce Eu³⁺ to Eu²⁺ or to remain in the divalent state of Mn²⁺. Both Eu²⁺ and Mn²⁺ were the doping ions in all phosphors studied in this project.

3.2 X-ray Diffraction

X-ray diffraction (XRD) uses the pattern produced by the diffraction of x-rays through the lattice of atoms in a material to reveal the nature (symmetric) structure of that lattice, which usually leads to an understanding of the structure of the material. The lattice constants of compounds are determined by using Bragg's law. The X-ray photons physically interact with the electrons that surround the atoms. X-rays scattered from a crystalline solid can constructively interfere, producing a diffraction pattern.

This technique works because in a crystalline material the inter-atomic distances are of the order of the wavelength of X-ray radiation (10^{-8} cm). As a result, X-ray radiation is diffracted by the electron clouds in the crystal structure. This gives us diffraction maxima which are dependent on the type of atoms, and their spacing and distribution. The X-ray diffraction technique, therefore, is not a technique that produces images. However, the electron density can be reconstructed using the diffraction pattern which is obtained from a periodic assembly of molecules in the crystal. Using this, a model can preliminarily be created. Then calculated diffractions can be compared with observational data, to finally have an accurate unambiguous 3D physical structure of the material.

3.3 Photoluminescence and Excitation

Excitation and photoluminescence spectra were measured at room temperature using a FluoroMax 2 spectrofluorometer. This spectrometer consists of a light source (a Xe lamp), slits, a monochromator, sample compartment, reference detector (photo diode), a spectrometer and a signal detector (PMT). Photoluminescence describes the process in which energy is emitted, in form of light, from a material at a different wavelength under excitation of a light source at which is absorbed by the sample.

In the case of the excitation spectrum the plot is actually an absorption spectrum which is obtained by monitoring the luminescence at a specific wavelength (at the peak of emission). The excitation spectrum is used to locate the energy levels of the excited states. In the monochromator, white light from a xenon lamp is collected by an elliptical mirror and directed to the entrance slit. Then the light is dispersed through the grating and then is

directed to the exit slit of the monochromator (for excitation). A specific wavelength is selected by the monochromator from the incoming light. The entrance and exit ports (or slits) of the spectrometer and the monochromator are adjustable in increments of 25 μ m. These are computer-controlled slits. To be able to detect the lamp profile of the output beam, a photodiode is used. The slits of the monochromator determine the amount of monochromatic light that is used to illuminate the sample. The spectrometer slits, on the other hand, control the intensity and resolution of the fluorescence signal that is detected by the photomultiplier (PMT). The PMT signals are amplified and processed.

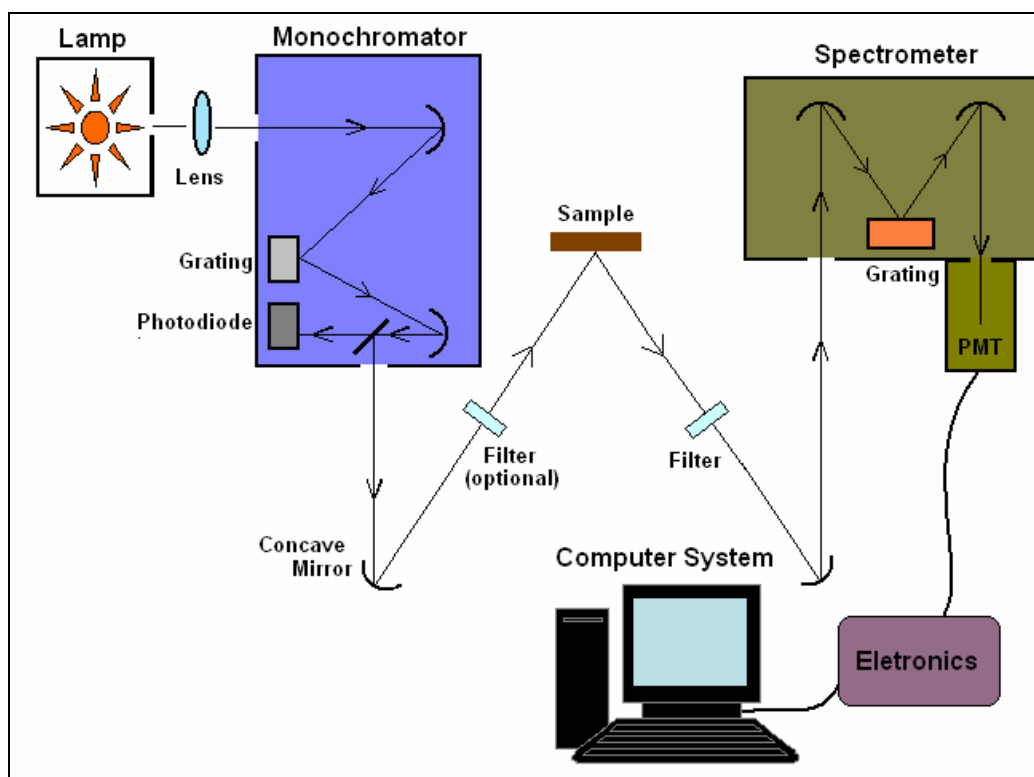


Figure 3 Schematic of the Fluoromax 2 System

In the measurements of luminescence spectroscopy with Fluoromax 2, the following issues have to be addressed:

a. Second order diffraction interference of the pump wavelength.

The diffraction relation of a grating is known to be:

$$d \sin \theta = m\lambda ,$$

d is the spacing of the adjacent ruled grooves of the grating, m is the order of the diffraction and θ is the angular direction of the diffraction. When the spectrometer is scanning, the $\sin \theta$ changes until the required wavelength of the signal is sent to the exit slit. Note that for the first order case, with wavelength λ , the signal will be overlapped with the second order of wavelength $\frac{\lambda}{2}$. To avoid this problem a cut-off filter is used between the sample and the entrance slit of the spectrometer.

For example, if you use 300nm of Xe lamp radiation to pump a sample and attempt to measure the emission in the spectral range of 500 – 700nm, the second order of the pump light (300nm) will appear at the wavelength 600nm. Without a cut-off filter to block the 300nm pump light, this light will give a huge peak at 600nm. This will not only make the scan failed, but also gives the risk of damaging the PMT.

b. Interference of the lamp background.

It is known that all the optical devices inside the instrument can produce strong diffuse scattering of the lamp output. Because the lamp illuminates the internal chamber of

the monochromator, the light output is always mixed with the background of the lamp. In other words sample that has a weak emission will have an emission spectrum mixed with a lamp profile in the background. For example, some emission spectra measured always show sharp peaks around 467nm. These peaks are known to come from the lamp output. In order to reduce this interference, a UV band-pass filter can be used. This filter only allows the excitation light with selected pump wavelength to reach the sample and rejects the rest of the lamp background which interferes with the fluorescence measurement.

c. Normalization of excitation spectrum for lamp profile.

The output of the xenon lamp is obviously a function of the wavelength. Therefore, a normalization of the excitation spectrum needs to be made. The relationship of the measured luminescence intensity of the sample $I(\lambda)$, the absorption $A(\lambda)$, the spectral response of the monochromator $M(\lambda)$ and the pump power of the lamp $L(\lambda)$ is given by:

$$I(\lambda) = M(\lambda)A(\lambda)L(\lambda).$$

From this relation we can obtain the excitation (absorption) spectrum:

$$A(\lambda) = \frac{I(\lambda)}{(M(\lambda)L(\lambda))} = I(\lambda) \cdot correction(\lambda) = \frac{I(\lambda)}{R_c}.$$

$I(\lambda)$ is the luminescent intensity measured by the PMT of the spectrometer and R_c is the corrected lamp signal detected by the photodiode of the monochromator unit.

d. Correction for Instrumentation spectral response.

The instrument (spectrofluorometer) sensitivity varies with wavelength due to the fact that in the spectrometer unit, diffraction efficiency of gratings, refractive indexes of lenses and the spectral response of the PMT, all depend on the wavelength. Therefore, the spectrum measured can be distorted. The wavelength dependence of the instrumentation is called the instrumentation spectral response, and has to be corrected. Mathematically we will have

$$S(\lambda) = E(\lambda)R(\lambda),$$

where S is the measured emission signal, E is the real emission spectrum and R is the instrumentation spectral response. Then the real emission spectrum of the materials is:

$$E(\lambda) = \frac{S(\lambda)}{R(\lambda)} = S(\lambda)C(\lambda).$$

The correction factor of the fluorospectrometer,

$$C(\lambda) = \frac{1}{R(\lambda)}$$

is pre-measured using a standard light source and is stored in a file called the correction function. When an emission spectrum is measured, an option of Sc, in the experiment screen, should be selected for corrected fluorescent spectrum.

3.4 Photoluminescence Measurements at Low-Temperature

Measurements are made with a SPEX 1403 Double Spectrometer, a Coherent Innova 306 Argon Laser and a He close cycle cryostat. The argon laser has an output at wavelength 351nm, 368nm, 457.9nm, 488nm and 515nm, which can be selected to pump the upper

excited state of rare earth ions in the phosphors. In all our measurements, the UV emission 351nm is used, to prevent the peak of the laser emission to appear in the spectrum to be measured. Samples were placed onto a cooling finger of the closed cycle He cryostat (RMC-Cryosystems) that provided temperatures from 8K to 300K. To achieve this range of temperatures an RMC CR31-21 Temperature Controller was used. The vacuum of the cryostat was achieved with a Vactronic mechanical pump.

4 SAMPLE PREPARATION

The samples were prepared, as we previously discussed, via chemical solid-state reaction. The samples, in a combustion boat, were pre-sintered and sintered at different temperatures in a Lindberg/Blue (500W) furnace. The pre-sintering process was done in an atmosphere of air and then sintered in an atmosphere of flowing $H_2 + 5\%N_2$ gas. Before the pre-sintering process, thorough mixing and mortaring all the materials for approximately 45 minutes were used. The powders are pressed into pellets and then the heating process was performed. After the pre-sintering process, the samples were ground for the second time for approximately 25 minutes and press into pellets. Then the last heating process was taken. The second grounding process is necessary in order to make the mixture homogeneous.

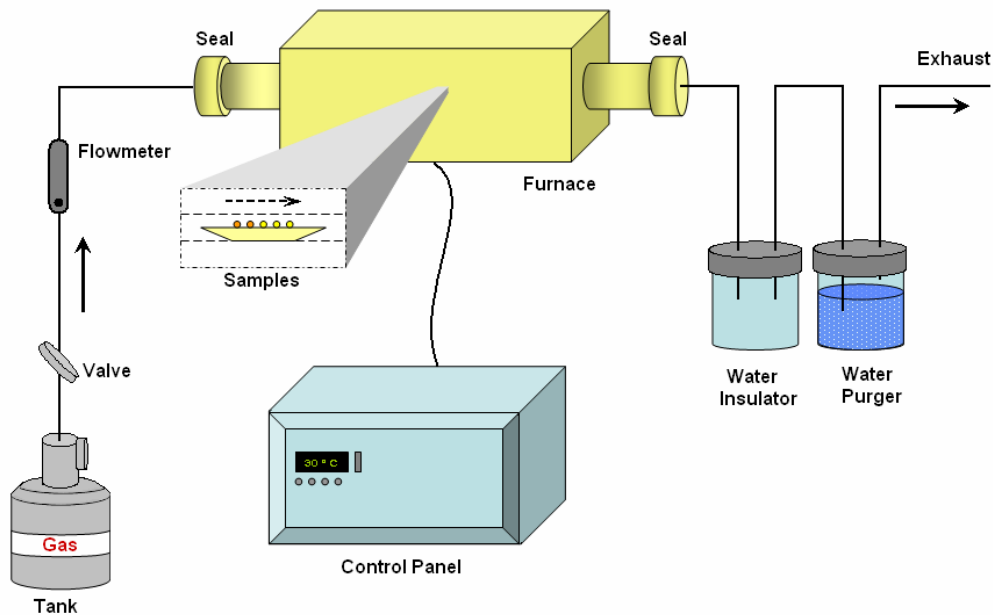
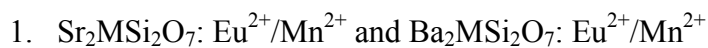


Figure 4 Schematic of the Firing-sample preparation

The three groups of materials that we have studied are as follows:



The furnace system used is shown in Figure 4 and it works with a temperature controller and a gas flow system. The exhaust gas flows and passes through a water container to purge the chemicals for environment safety. Typically a good heating process will be long enough to get the chemical reaction completed, but not too long to cause chemical loss through evaporation.

5 SPECTROSCOPY OF PHOSPHATES

5.1 Sample Preparation Details

The Mn^{2+} single doped and $\text{Mn}^{2+}/\text{Eu}^{2+}$ double doped $\text{Mg}_2\text{P}_2\text{O}_7$, $\text{Ca}_2\text{P}_2\text{O}_7$ and $\text{Sr}_2\text{P}_2\text{O}_7$ were prepared according to the following recipes:



where M= Sr, Ca, and Mg.

An extra 2% of P_2O_5 is added in order to compensate for the loss of P_2O_5 due to vaporization during the sintering period. The samples were pre-sintered at 600°C for 2 hours and sintered at $1,100^\circ\text{C}$ for an hour.

5.2 X-ray Diffraction

The X-ray diffraction measurements were made at room temperatures in the scattering range of $10.000^\circ - 70.000^\circ$ at steps of 0.010° in 2θ using a Siemens D-5000 X-ray diffractometer in the X-ray laboratory of the Geology Department. XRD patterns of $\text{Mg}_2\text{P}_2\text{O}_7$, $\text{Ca}_2\text{P}_2\text{O}_7$ and $\text{Sr}_2\text{P}_2\text{O}_7$ are shown in Fig. 5, 6 and 7, respectively. The result of $\text{Ca}_2\text{P}_2\text{O}_7$ demonstrates that the sample is not well crystallized. The result of $\text{Mg}_2\text{P}_2\text{O}_7$ shows very good crystalline structure.

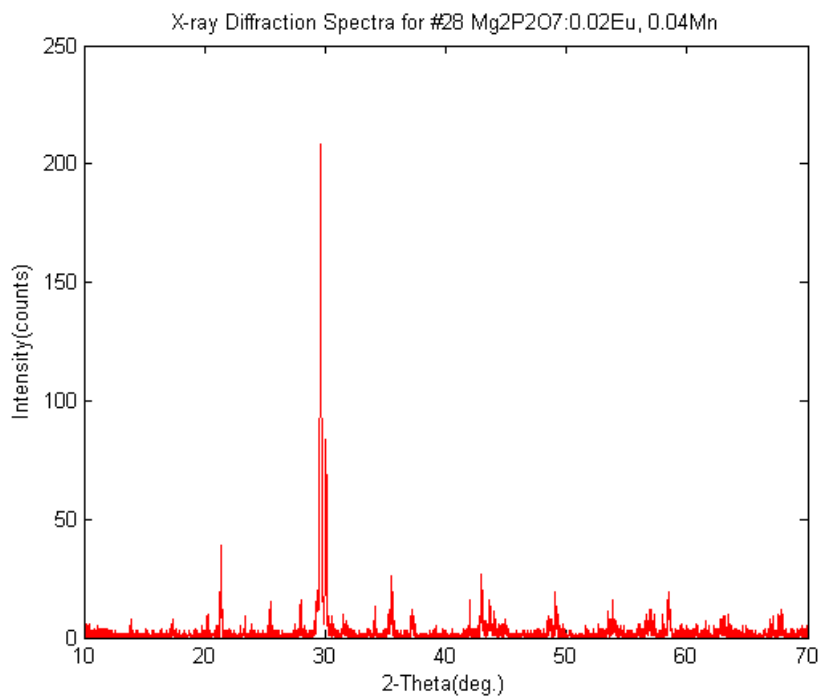


Figure 5 XRD Pattern for Mg₂P₂O₇

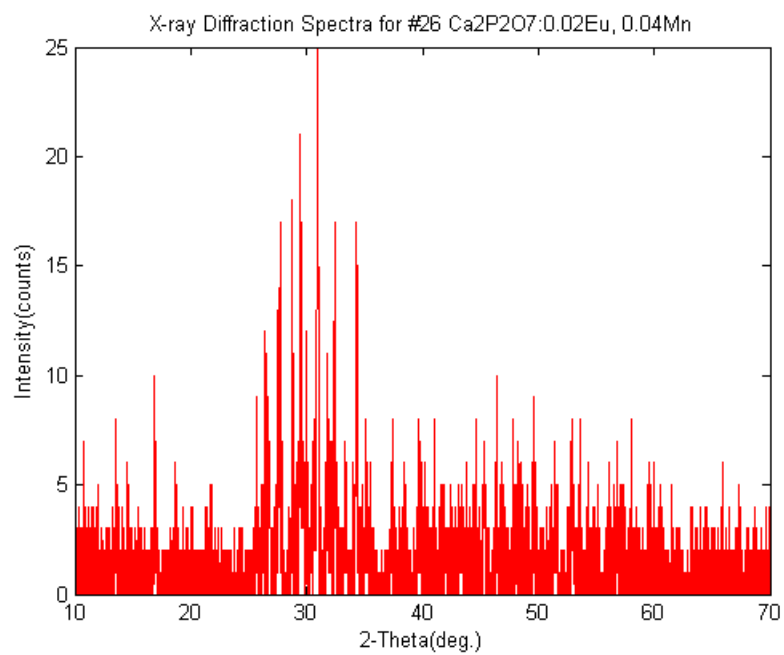


Figure 6 XRD Pattern for Ca₂P₂O₇

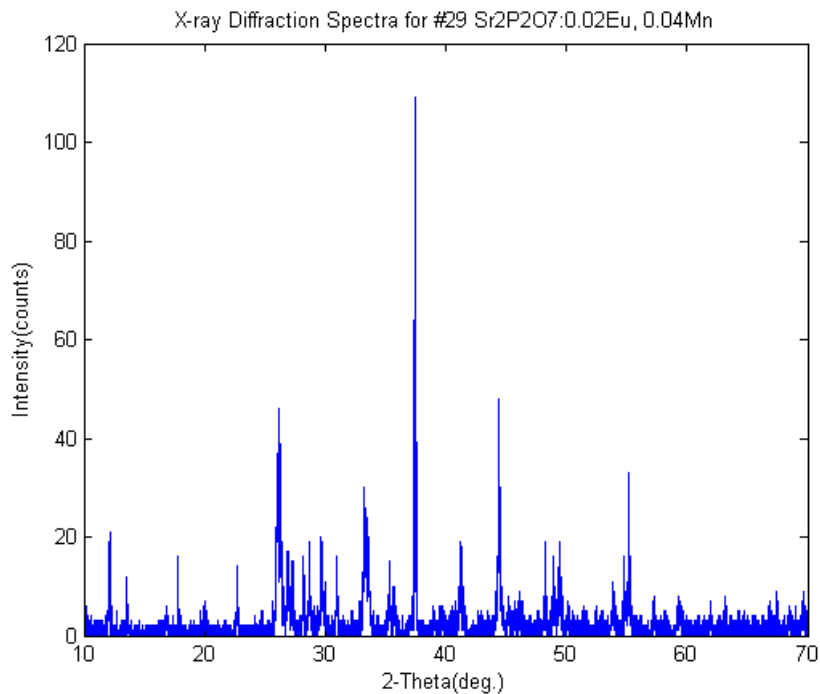


Figure 7 XRD Pattern for $\text{Sr}_2\text{P}_2\text{O}_7$

5.3 Excitation and Luminescence Spectra

5.3.1 $\text{Mg}_2\text{P}_2\text{O}_7$

The emission spectrum of Mn^{2+} doped $\text{Mg}_2\text{P}_2\text{O}_7$ is shown in Figure 8 in the spectral range of 450-800nm. A broad emission band is peaked at 675nm. The band rides on a lamp profile, and the peak position may be shifted to the longer wavelength (see spectrum of $\text{Mg}_2\text{P}_2\text{O}_7:\text{Eu}^{2+}, \text{Mn}^{2+}$).

In Figure 8, the excitation spectrum, for $\text{Mg}_2\text{P}_2\text{O}_7:0.02\text{Mn}^{2+}$ is also shown. Absorption bands at 345, 360 and 410, 430 and 515nm, are observed. 410nm peak appears to be the strongest.

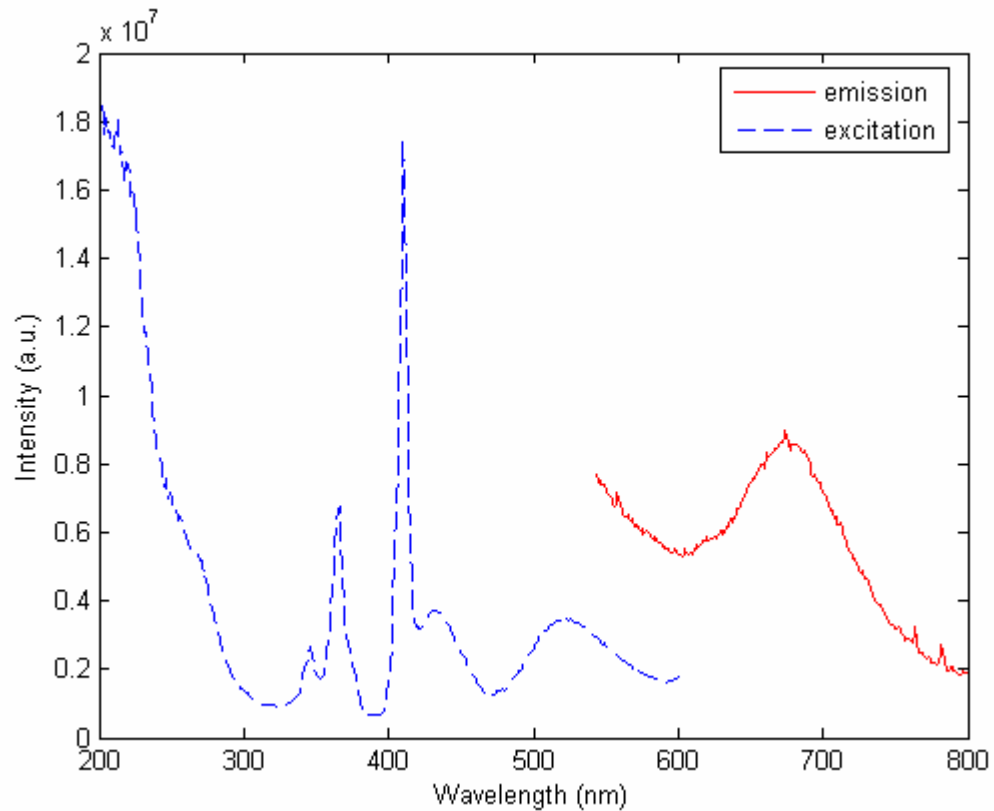


Figure 8 Luminescence ($\lambda_{ex} = 410\text{nm}$) and Excitation ($\lambda_{em} = 675\text{nm}$) Spectrum of $\text{Mg}_2\text{P}_2\text{O}_7:0.02\text{Mn}$

Figure 9 shows the emission and excitation spectra of $\text{Mg}_2\text{P}_2\text{O}_7: 2\%\text{Eu}^{2+}, 4\%\text{Mn}^{2+}$. In addition to the red emission band at 656nm from Mn^{2+} , a very strong emission band at 448nm is observed. This violet emission band is from $5d$ state of Eu^{2+} . The excitation spectrum, monitoring the Mn^{2+} emission at 680nm, is also shown in the figure also. The broadband centered at 300nm with some shoulders near 280nm and 350nm is the absorption transition from ^8S ground state to the $5d$ state of Eu^{2+} . Weak peaks at 410, 430 and 515nm, barely seen in the excitation spectrum, originated from Mn^{2+} , as indicated in the excitation spectrum of Mn^{2+} doped $\text{Mg}_2\text{P}_2\text{O}_7$ shown in Fig. 8. This result reveals that a strong and

efficient energy transfer occurs from Eu^{2+} to Mn^{2+} . $5d$ absorption transition of Eu^{2+} makes the dominant contribution of the red emission absorption of Mn^{2+} over the direct absorption by Mn^{2+} itself.

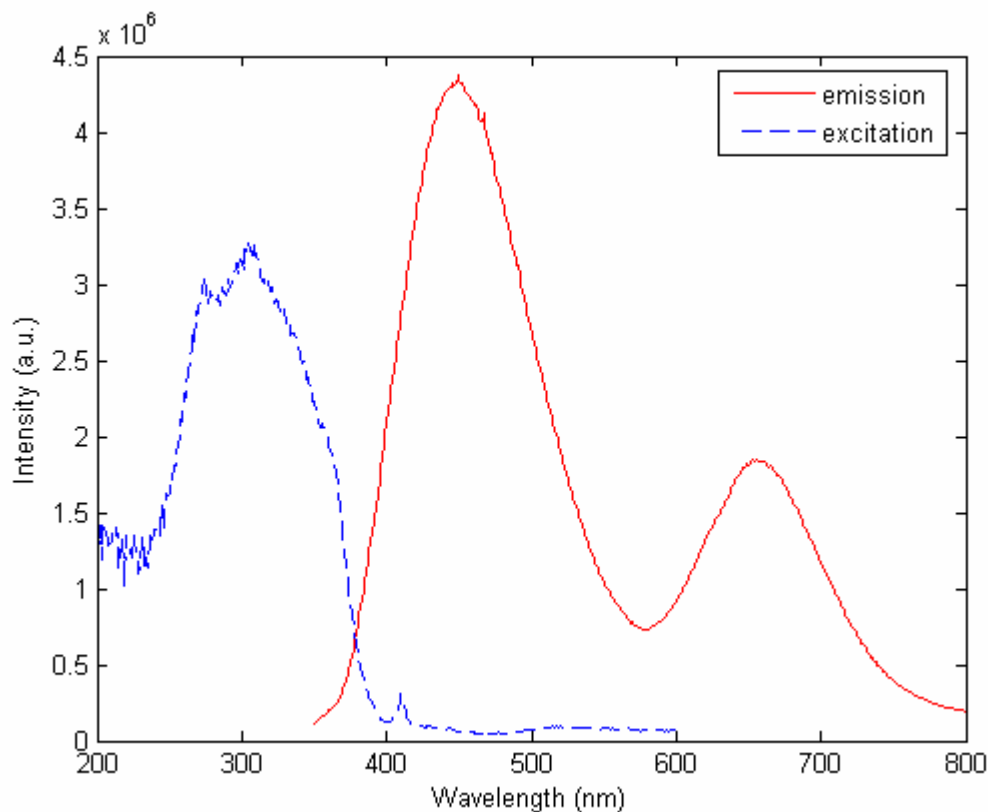


Figure 9 Luminescence ($\lambda_{ex} = 305\text{nm}$) and Excitation ($\lambda_{em} = 680\text{nm}$) Spectrum of $\text{Mg}_2\text{P}_2\text{O}_7:0.02\text{Eu}, 0.04\text{Mn}$

5.3.2 $\text{Ca}_2\text{P}_2\text{O}_7: 0.02\text{Eu}, 0.04\text{Mn}$

The emission of $\text{Ca}_2\text{P}_2\text{O}_7:\text{Mn}^{2+}$ is too weak to be seen because of poor crystalline structure. For the sample $\text{Ca}_2\text{P}_2\text{O}_7:\text{Eu}^{2+}, \text{Mn}^{2+}$, the emission spectrum pumped at 305nm is

shown at Fig. 10. Two broad peaks at 422nm and 562nm were observed. They are due to Eu^{2+} and Mn^{2+} , respectively. The excitation spectrum is also measured by monitoring the Mn^{2+} emission at 580nm. As in the case of $\text{Mg}_2\text{P}_2\text{O}_7:\text{Eu}^{2+}, \text{Mn}^{2+}$ the broad UV band is the $5d$ transition of Eu^{2+} , while the weak background from 400-500nm is related with the weak absorption of Mn^{2+} . Because of efficient energy transfer, the red emission of Mn^{2+} could be observed when the Eu^{2+} ions were pumped at 305nm.

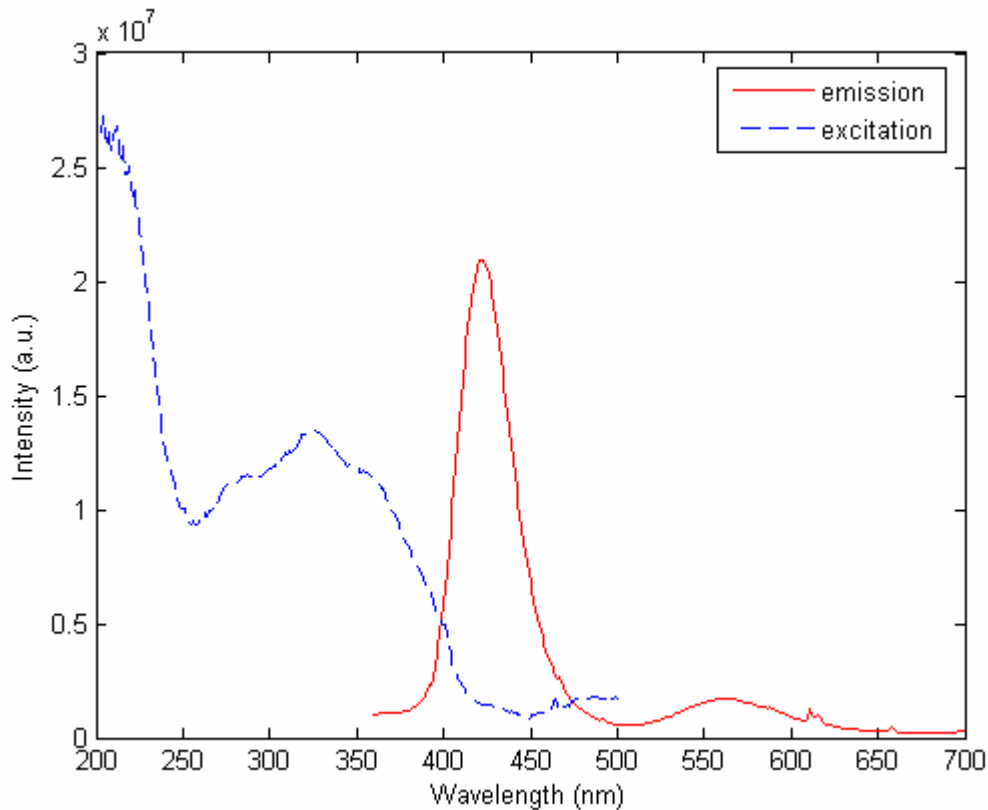


Figure 10 Luminescence ($\lambda_{ex} = 368\text{nm}$) and Excitation ($\lambda_{em} = 580\text{nm}$) Spectrum of $\text{Ca}_2\text{P}_2\text{O}_7:0.02\text{Eu}, 0.04\text{Mn}$

5.3.3 $Sr_2P_2O_7: 0.02Eu, 0.04Mn$

Similar to the case of $Ca_2P_2O_7$ the emission of Mn^{2+} single doped sample is very weak and is buried in the lamp's background. However, strong emission bands at 420nm and 560nm were found when the sample was pumped at 300nm in the sample $Sr_2P_2O_7:Eu^{2+}, Mn^{2+}$. The two emission bands are corresponding to the $5d$ transition of Eu^{2+} and the 4T_2 transition of Mn^{2+} , respectively. The excitation spectrum shows triple peaks at 275, 345 and 360nm.

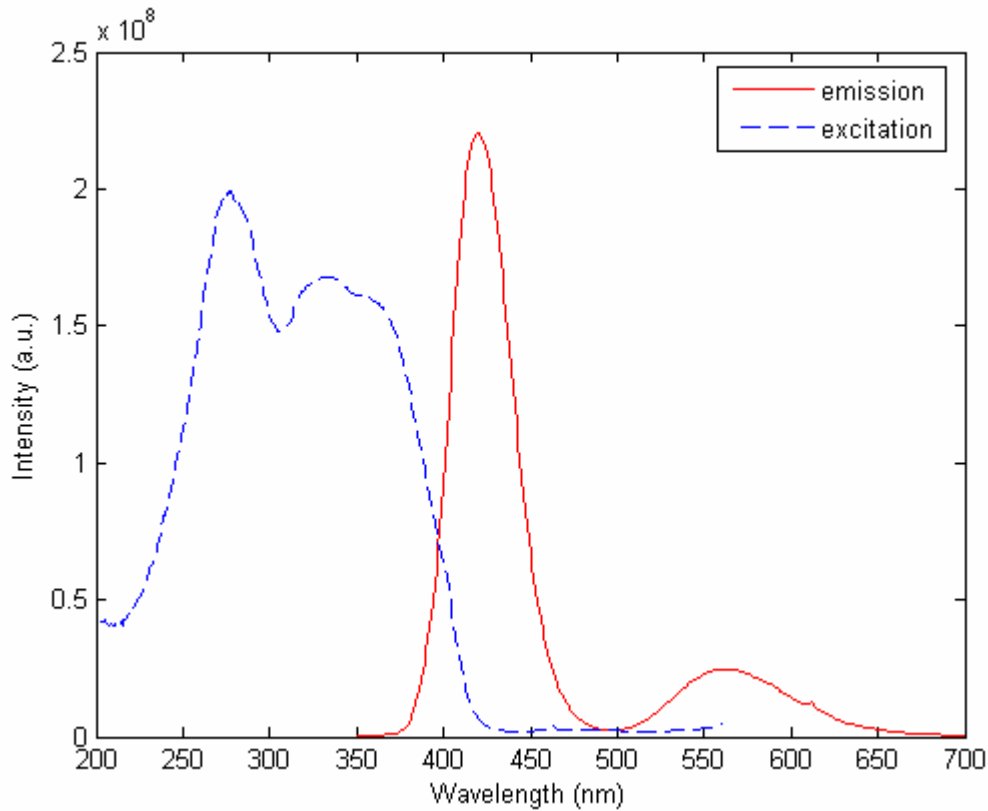


Figure 11 Luminescence ($\lambda_{ex} = 300nm$) and Excitation ($\lambda_{em} = 580nm$) Spectrum of $Sr_2P_2O_7:0.02Eu, 0.04Mn$

5.4 Discussion: Mn²⁺ Electronic Configuration

5.4.1 *Electronic Configuration*

Mn²⁺ has 3d⁵ electronic configuration. For a free ion, the ground state is ⁶S, in which the total orbital quantum number L = 0 and all spins of the five electrons are parallel, resulting in the total spin S = $\frac{5}{2}$ and having a spin degeneracy of 2s + 1 = 6. The first excited state of the free ion is a ⁴G state, the next higher excited states are ⁴P, ⁴D, ²I, and ⁴F. In the crystal field of octahedron sites, the ground state is labeled as ⁶A₁. The ⁴G (L = 4) state is split into ⁴T₁, ⁴T₂ and ⁴A₁ + ⁴E. As shown in the Sugano-Tanabe diagram in Figure 12. It is interesting to note that, with increasing the strength of the crystal field, the energy separation of both ⁴T₁ and ⁴T₂ states to the ground state decreases. Theoretically, the crystal field of tetrahedral is only $\frac{4}{9}$ of that of octahedral. As a result, Mn²⁺ in a tetrahedron site has emission at a shorter wavelength, and it used to be green. In contrast, Mn²⁺ in an octahedron site has emission at a longer wavelength, and it used to be orange or red. In other words, the emission wavelength of Mn²⁺ can be tuned by selecting crystal field of lattice sites and crystal hosts.

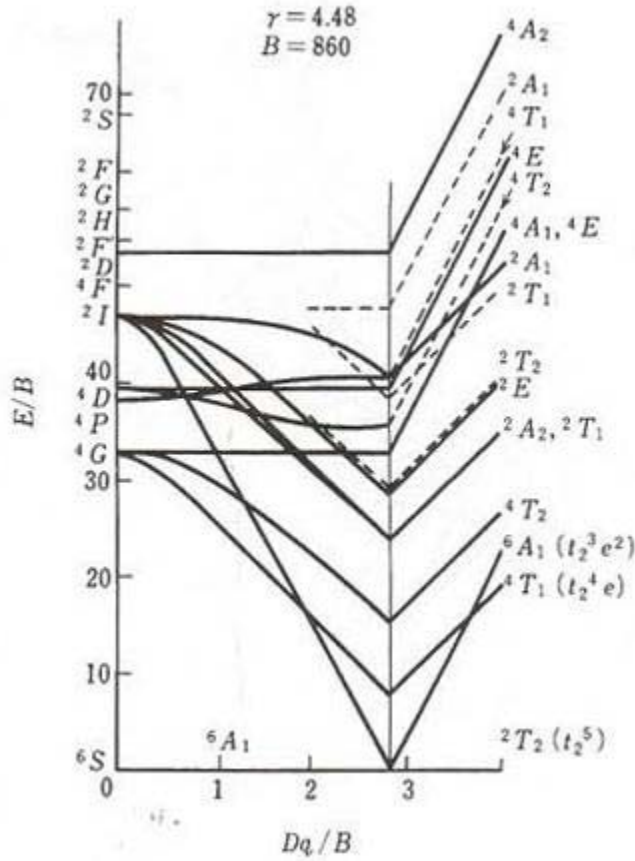


Figure 12 Sugano-Tanabe diagram (from Shionoya and Yen 1999)

5.4.2 Assignment of Energy Levels of Excitation Spectrum of Mn^{2+}

Compared with the Sugano-Tanabe diagram in Figure 12, the absorption peaks in the excitation spectrum of $M_2P_2O_7:Mn^{2+}$ shown above can be assigned as follow: 515nm \rightarrow $4T_1(4G)$; 430nm \rightarrow $4T_2(4G)$; 410nm \rightarrow $4E(4G)$, $4A(4G)$; 360nm \rightarrow $4T_2(4D)$, $4E(4D)$; 345nm \rightarrow $4T_1(4P)$; and 260nm \rightarrow $4A_2(4F)$, $4T_1(4F)$. The emission from $2T_2(2I)$ is very weak and can be only observed at very low-temperature transition at 656nm. Compared with the absorption

peak of ${}^4T_1({}^4G)$ at 515nm. The emission of the state at 656nm gives an observed Stoke shift of 4167cm^{-1} .

5.4.3 *Selection Rule*

As shown in the Sugano-Tanabe diagram of $3d^5$ the ground state of Mn^{2+} has six manifold spin degeneracy. However, no excited states of Mn^{2+} have sixlet spin degeneracy. As a result, all the absorption transitions to the excited state are spin forbidden, and they used to be quite weak. In order to increase the emission intensity, a sensitizer has to be used to increase the excitation of Mn^{2+} ions.

5.4.4 *Energy Transfer and Sensitization*

As mentioned before, the emission of Mn^{2+} in all phosphates can be efficiently sensitized through energy transfer from Eu^{2+} to Mn^{2+} . The optical transition, between $5d$ state and the ground state 8S of Eu^{2+} is both electric dipole and spin allowed. This transition is very strong.

From the excitation spectrum, measured by monitoring the Mn^{2+} emission at 656nm, it can be seen that the contribution of Eu^{2+} to the Mn^{2+} emission (the over all area of the UV peaks) is thousands of times larger than the direct excitation of Mn^{2+} at 410nm peak, which is the strongest absorption as shown in Figure 8.

Theoretically, the energy transfer rate between two ions depends on the overlapping integral:

$$R = \int E(Eu, \lambda) \cdot A(Mn, \lambda) d\lambda ,$$

where $E(Eu, \lambda)$ is the emission spectrum of the donor (in this case is Eu^{2+}) and $A(Mn, \lambda)$ is the absorption spectrum of the acceptor (in this case is Mn^{2+}).

From Figure 9, it can be seen that, the emission band of Eu^{2+} at 448nm is well overlapped with the absorption bands of Mn^{2+} at 410, 430 and 515nm. Therefore, an efficient energy transfer is expected.

It should be pointed out that the electronic process of energy transfer is not a simple emission-reabsorption process. As mentioned above, absorption probability of Mn^{2+} is very weak. A simple emission-re-absorption process can not give an efficient and fast energy transfer from Eu^{2+} to Mn^{2+} . The process should be a direct excitation transfer through a quantum interaction between the two ions.

5.4.5 *Evaluation of the Phosphate Phosphors*

The emission wavelength of Eu^{2+} in $Ca_2P_2O_7$ and $Sr_2P_2O_7$ is too short (too violet). They are not interesting for LED applications. The emission of Mn^{2+} in the two phosphors has green color. They are not important to applications either.

In contrast, $Mg_2P_2O_7:Eu^{2+}, Mn^{2+}$ is a very interesting phosphor, the blue emission at 448nm and red emission at 656nm are quite suitable form LED tricolor phosphor devices. Under UV excitation, this phosphor can produce two basic colors: blue and red. If combining with a green phosphor a white light source can be constructed. Adjusting the concentration of Mn^{2+} , the red component can be increased to give better color rendering to the LED devices.

Luminescence Center	Chemical Composition	Peak wavelength (nm)	Luminescence Color
Mn ²⁺	Mg ₂ P ₂ O ₇ :0.02 Mn (#24)	675	Red
Eu ²⁺ , Mn ²⁺	Ca ₂ P ₂ O ₇ :0.02Eu, 0.04Mn (#26)	(422), 562	Red
	Mg ₂ P ₂ O ₇ :0.02Eu, 0.04Mn (#28)	(448), 656	Red
	Sr ₂ P ₂ O ₇ :0.02Eu, 0.04Mn (#29)	392, (420), 560	Blue

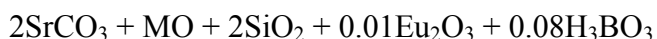
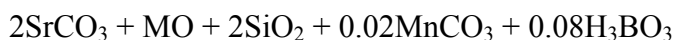
Table 2 Results for the Phosphates (the wavelength in parenthesis is the strongest peak)

6 SPECTROSCOPY OF SILICATES

It has been reported (Lehman 1978) that $\text{Ca}_2\text{MgSi}_2\text{O}_7:\text{Eu}^{2+}, \text{Mn}^{2+}$ has two emission bands at 541nm from Eu^{2+} and 689nm from Mn^{2+} . In this work, Eu^{2+} and Mn^{2+} doped $\text{Sr}_2\text{MgSi}_2\text{O}_7$, $\text{Sr}_2\text{ZnSi}_2\text{O}_7$ and $\text{Ba}_3\text{ZnSi}_2\text{O}_8$ are investigated.

6.1 Sample Preparation Details

Eu^{2+} or Mn^{2+} single doped and $\text{Mn}^{2+}/\text{Eu}^{2+}$ double-doped $\text{Sr}_2\text{MgSi}_2\text{O}_7$, $\text{Sr}_2\text{ZnSi}_2\text{O}_7$, $\text{Ba}_2\text{ZnSi}_2\text{O}_7$, $\text{Ba}_3\text{MgSi}_2\text{O}_8$, $\text{Ba}_2\text{MgSi}_2\text{O}_7$ and $\text{Ba}_3\text{ZnSi}_2\text{O}_8$ were prepared. The samples were prepared according to the following recipes:



where M= Mg, Zn.

For Ba-silicates 2SrCO_3 is replaced by 2BaCO_3 (or 3BaCO_3 for $\text{Ba}_3\text{MgSi}_2\text{O}_8$). H_3BO_3 is used as a flux to get better chemical reaction.

6.2 Excitation and Luminescence Spectra

6.2.1 $\text{Sr}_2\text{MgSi}_2\text{O}_7:4\%\text{Eu}^{2+}, 8\%\text{Mn}^{2+}$

The excitation and emission spectra of $\text{Mn}^{2+}/\text{Eu}^{2+}$ double-doped $\text{Sr}_2\text{MgSi}_2\text{O}_7$ are shown in Figure 13. Two emission bands were observed at 458nm and 670nm, which originates from Eu^{2+} and Mn^{2+} , respectively. In the excitation spectrum, monitoring Eu^{2+} emission at 457nm, there are two overlapped bands at 290nm and 374nm. These bands are the absorption transition of $5d$ states of Eu^{2+} . Excitation spectrum monitoring the Mn^{2+} emission at 670nm was also measured. The result demonstrates that almost all the red emission of Mn^{2+} is the result of energy transferred from the excitation of Eu^{2+} .

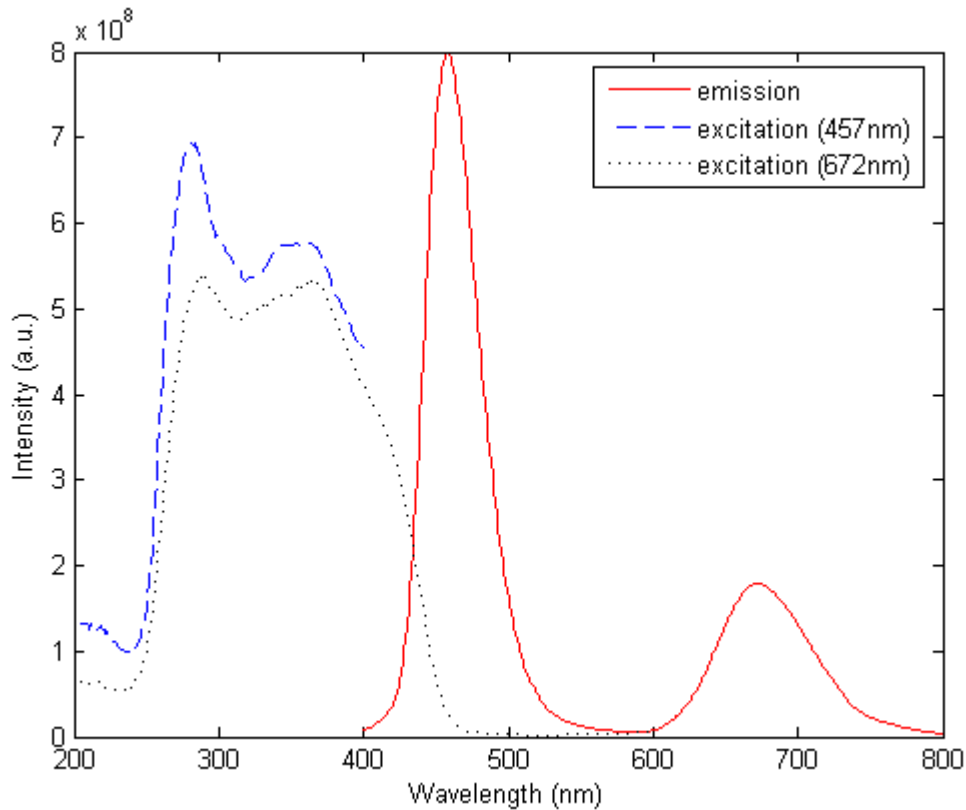


Figure 13 Luminescence ($\lambda_{ex} = 350\text{nm}$) and Excitation ($\lambda_{em} = 457\text{nm}$ and 672nm) Spectra of $\text{Sr}_2\text{MgSi}_2\text{P}_2\text{O}_7:4\%\text{Eu}^{2+}, 8\%\text{Mn}^{2+}$

6.2.2 $Ba_2MgSi_2O_7:4\%Eu^{2+},8\%Mn^{2+}$

Phosphor $Ba_2MgSi_2O_7:Eu^{2+},Mn^{2+}$ was also investigated. Although, the chemical formula is similar to $Sr_2MgSi_2O_7$, the emission spectrum is quite different from the later. The emission band actually consists of two overlapped peaks at 495 and 520nm as shown in Figure 14. The 495nm bands come from Eu^{2+} substituted at Sr site, while 520nm peak is from Mn^{2+} at Mg sites. The excitation spectrum consists of three overlapped bands at 285, 355 and 410nm. Under UV excitation from 260 - 420nm, the sample shows a very bright green emission. It can be concluded that very efficient energy transfer occurs from Eu^{2+} to Mn^{2+} .

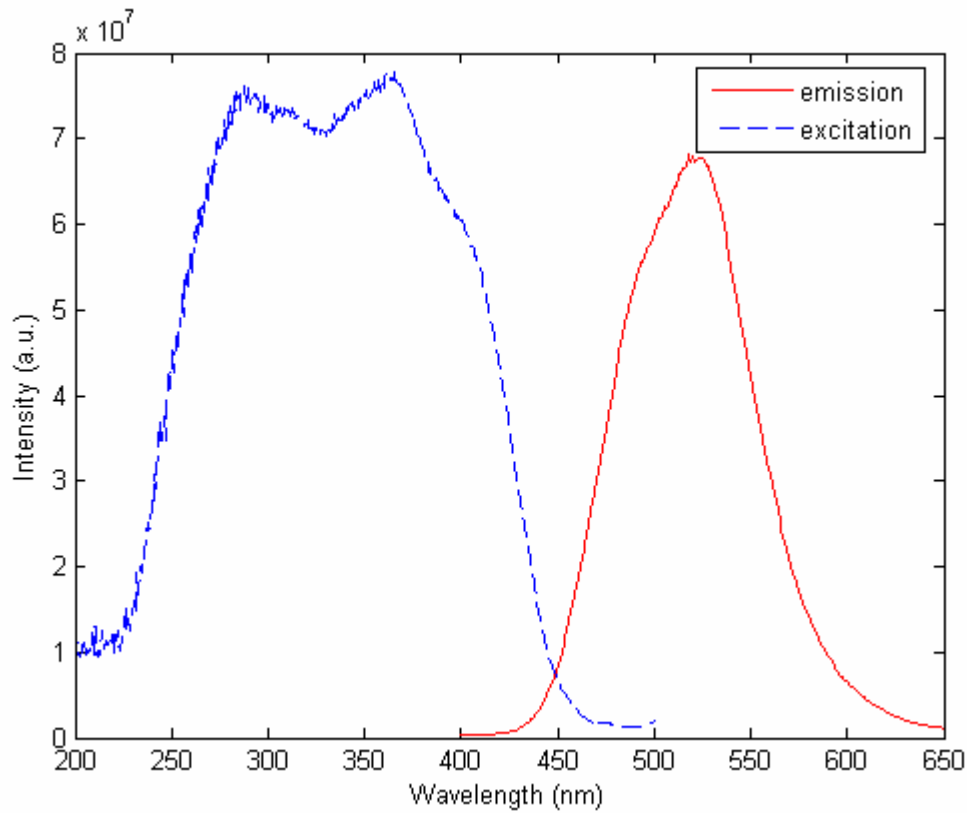


Figure 14 Luminescence ($\lambda_{ex} = 330\text{nm}$) and Excitation ($\lambda_{em} = 520\text{nm}$) Spectrum of $\text{Ba}_2\text{MgSi}_2\text{O}_7:4\%\text{Eu}^{2+}, 8\%\text{Mn}^{2+}$

6.2.3 $\text{Ba}_2\text{ZnSi}_2\text{O}_7:4\%\text{Eu}^{2+}, 8\%\text{Mn}^{2+}$; $\text{Ba}_2\text{ZnSi}_2\text{O}_7:\text{Eu}^{2+}$

In $\text{Ba}_2\text{MgSi}_2\text{O}_7$, Mg can be replaced by Zn. The emission and excitation spectra of $\text{Ba}_2\text{ZnSi}_2\text{O}_7:\text{Eu}^{2+}$ are presented in Figure 15. A broad band is located at 505nm. Compared with Eu^{2+} emission in $\text{Ba}_2\text{MgSi}_2\text{O}_7$, the band is shifted to longer wavelength by 10nm.

For $\text{Mn}^{2+}/\text{Eu}^{2+}$ double-doped $\text{Ba}_2\text{ZnSi}_2\text{O}_7$, the emission band appears at 555nm much broader than the emission band of $\text{Ba}_2\text{MgSi}_2\text{O}_7:\text{Eu}^{2+}$. It is believed that the broadband are

two well overlapped emission bands from both Eu^{2+} and Mn^{2+} . In other words, the emission band is not only from Mn^{2+} , nor only from Eu^{2+} , but from both of them.

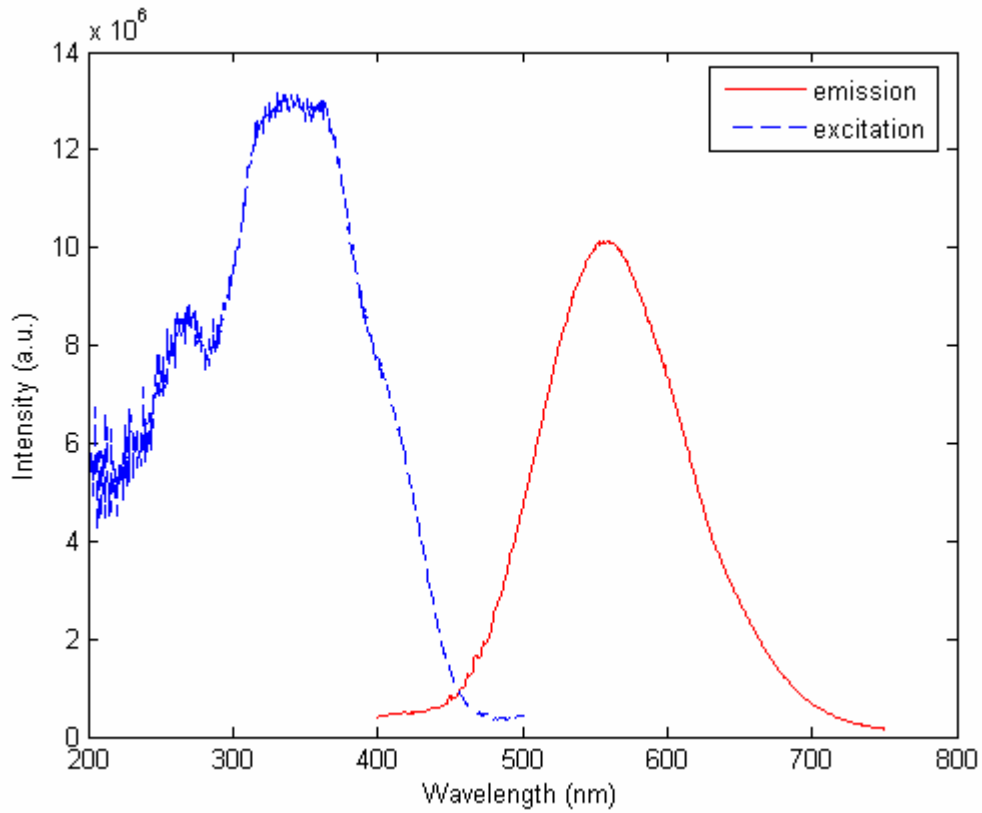


Figure 15 Luminescence ($\lambda_{ex} = 342\text{nm}$) and Excitation ($\lambda_{em} = 515\text{nm}$) Spectrum of $\text{Ba}_2\text{ZnSi}_2\text{O}_7:\text{Eu}^{2+}, \text{Mn}^{2+}$

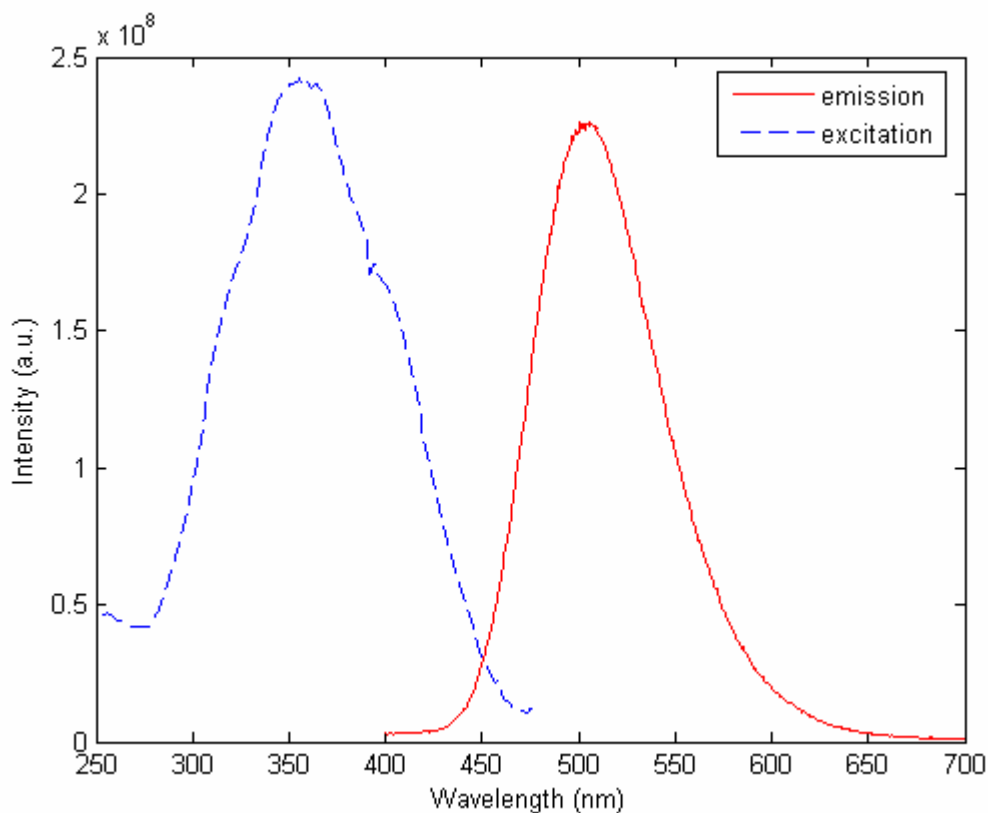


Figure 16 Luminescence ($\lambda_{ex} = 355\text{nm}$) and Excitation ($\lambda_{em} = 320\text{nm}$) Spectrum of $\text{Ba}_2\text{ZnSi}_2\text{O}_7:\text{Eu}^{2+}$

6.2.4 $\text{Ba}_3\text{ZnSi}_2\text{O}_8:4\%\text{Eu}^{2+},8\%\text{Mn}^{2+}; \text{Eu}^{2+}/\text{Mn}^{2+}$

Since the strong green emission of $\text{Ba}_2\text{ZnSi}_2\text{O}_7:4\%\text{Eu}^{2+}, 8\%\text{Mn}^{2+}$ is very interesting, we extended our study to tri-barium, zinc silicates. Figure 17 presents the emission and excitation spectra of $\text{Ba}_3\text{ZnSi}_2\text{O}_8:\text{Mn}^{2+}$. It is interesting to note that strong emission bands appear at the violet range and a weak broadband appears around 480nm. The broad 480nm weak band may be emission from Mn^{2+} at very low field site. The violet emission of 370 and 410nm bands are possibly from defect levels of the host. The excitation band at 320nm is the absorption of the defect.

The emission and excitation spectra of $\text{Ba}_3\text{ZnSi}_2\text{O}_8:\text{Eu}^{2+}$ are shown in Figure 18. A broad emission band is located at 505nm. The sharp structures near 612nm are emission peaks of residual Eu^{3+} of the sample, in which reduction of Eu^{3+} ions to Eu^{2+} may not be completed.

In the double-doped system, $\text{Ba}_3\text{ZnSi}_2\text{O}_8:4\%\text{Eu}^{2+}, 8\%\text{Mn}^{2+}$, only a single emission band near 505nm was observed under UV excitation at 310nm, as shown in Figure 19. This emission band is certainly related only with Eu^{2+} . At a low field site, the ${}^4\text{T}_1({}^4\text{D})$ state of Mn^{2+} might be higher than the lowest $5d$ energy component (see Figure 17, in which Mn^{2+} shows emission band near 480nm). As a result, photo-energy transfer from Mn^{2+} to Eu^{2+} may occur, but it will be very weak and negligible. As mentioned before, Mn^{2+} does not absorb photo-energy efficiently due to the limitation of the spin selection rule.

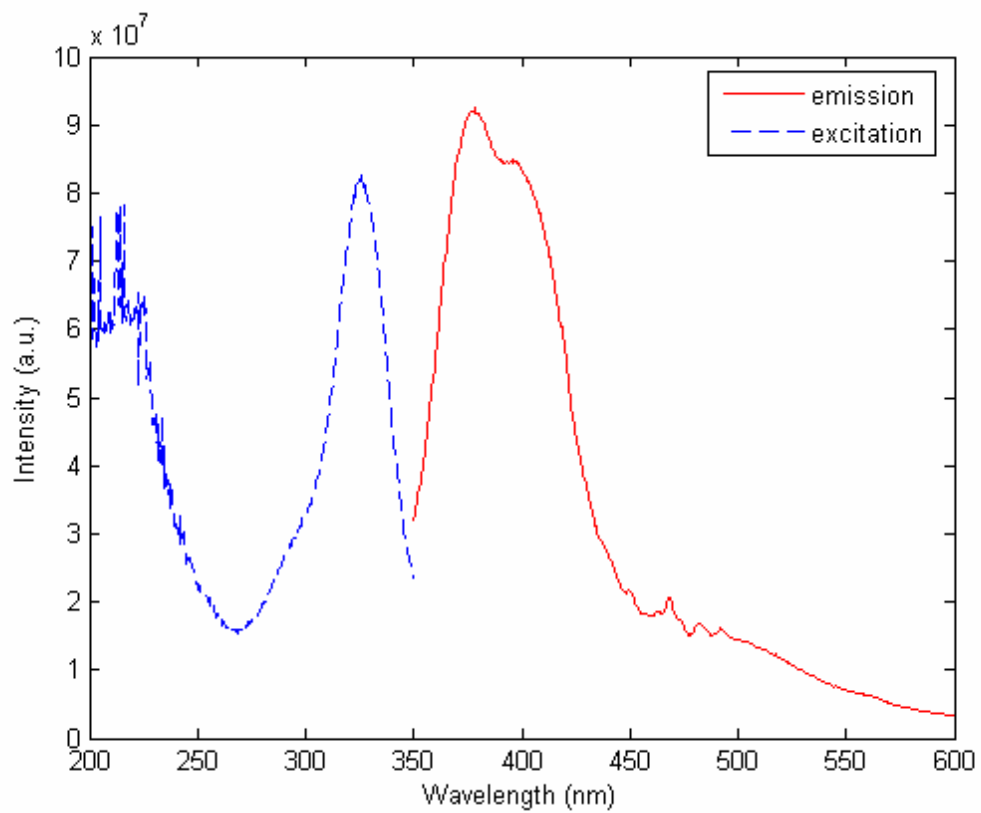


Figure 17 Luminescence ($\lambda_{ex} = 300\text{nm}$) and Excitation ($\lambda_{em} = 375\text{nm}$) Spectrum of $\text{Ba}_3\text{ZnSi}_2\text{O}_8:\text{Mn}^{2+}$

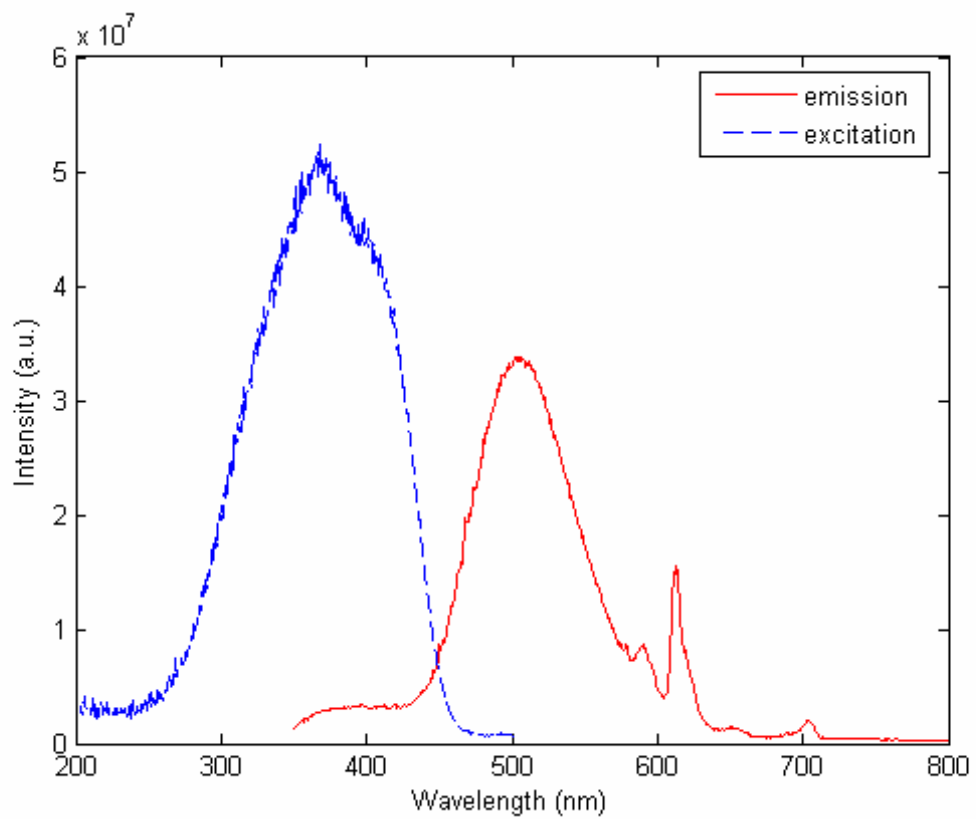


Figure 18 Luminescence ($\lambda_{ex} = 272\text{nm}$) and Excitation ($\lambda_{em} = 503\text{nm}$) Spectrum of $\text{Ba}_3\text{ZnSi}_2\text{O}_8:\text{Eu}^{2+}$

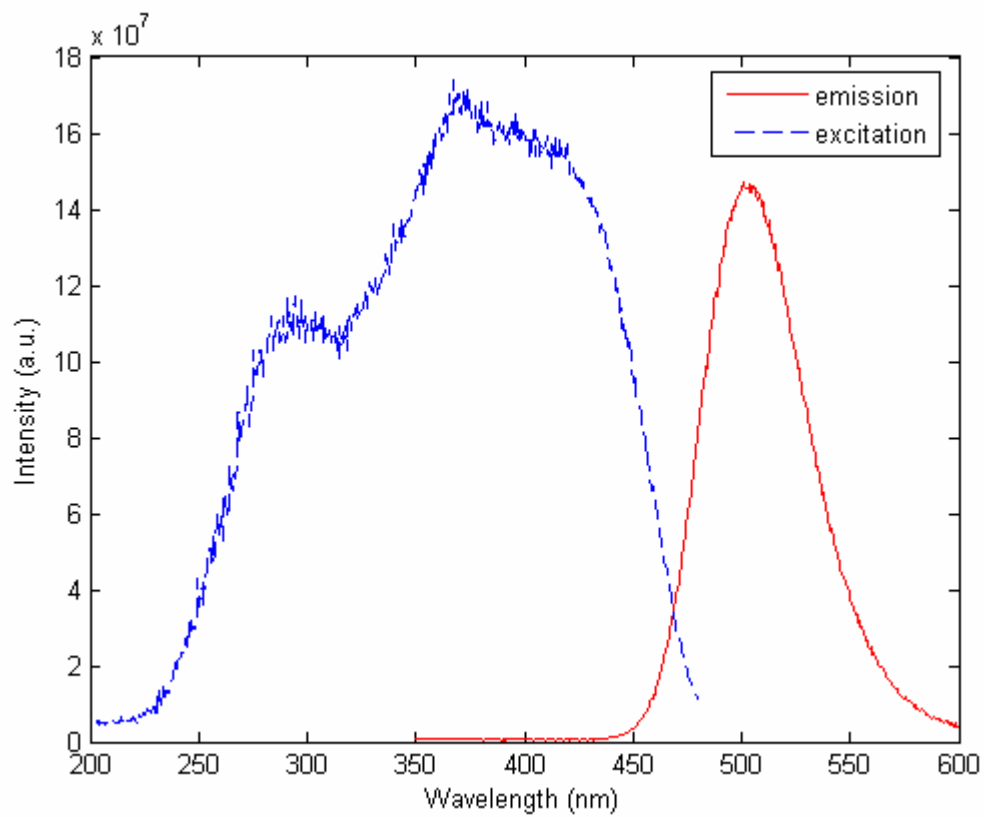


Figure 19 Luminescence ($\lambda_{ex} = 310\text{nm}$) and Excitation ($\lambda_{em} = 500\text{nm}$) Spectrum of $\text{Ba}_3\text{ZnSi}_2\text{O}_8:4\%\text{Eu}^{2+}, 8\%\text{Mn}^{2+}$

6.3 Low-Temperature Luminescence Spectra

6.3.1 $Sr_2MgSi_2O_7:4\%Eu^{2+}, 8\%Mn^{2+}$

The low-temperature luminescent spectrum of $Sr_2MgSi_2O_7:Eu^{2+}, Mn^{2+}$ was measured with a SPEX double spectrometer 1403. The sample was pumped using the 351nm line emission of an Ar laser. The luminescence spectrum consists of two peaks as shown in Figure 20. The first peak around 480nm is due to Eu^{2+} transition, and a slight blue-shift was observed upon heating. In the other hand the second peak (695nm) caused by transitions of Mn^{2+} ions showed a blue-shift of 20nm.

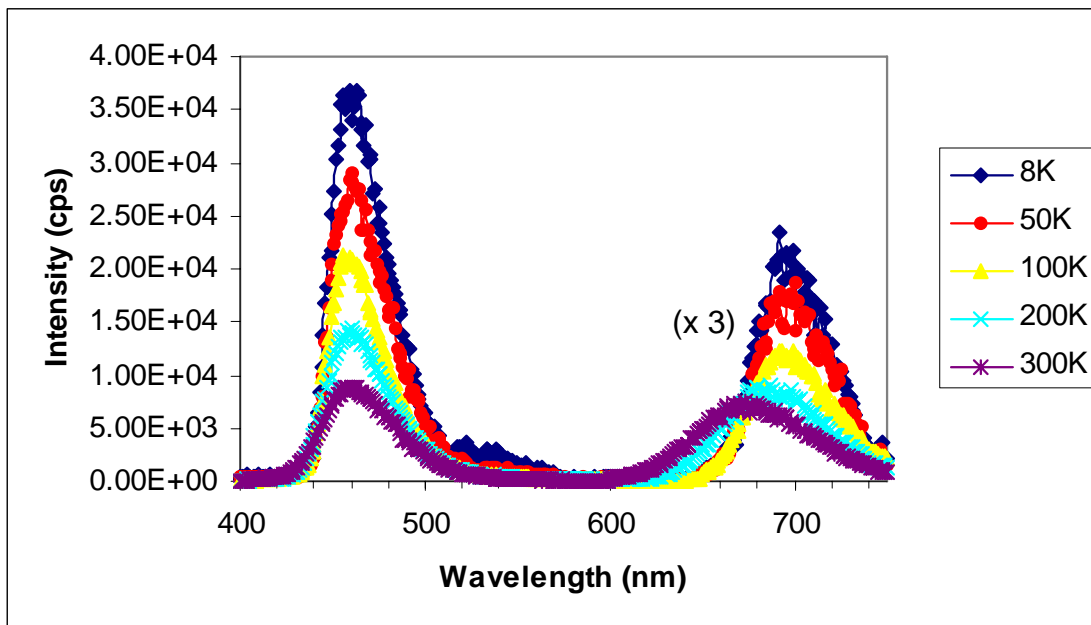


Figure 20 Low-temperature Luminescence Spectra of $Sr_2MgSi_2O_7:4\%Eu^{2+}, 8\%Mn^{2+}$

6.3.2 $Ba_2ZnSi_2O_7:Eu^{2+}$

The low-temperature luminescent spectrum of $Ba_2ZnSi_2O_7:Eu^{2+}$ was also measured. The sample was pumped using the same conditions discussed in section 6.3.1. The luminescence spectrum consisted of a broad peak at 525nm. A blue-shift of 30nm with increasing temperature was observed as shown in Figure 21.

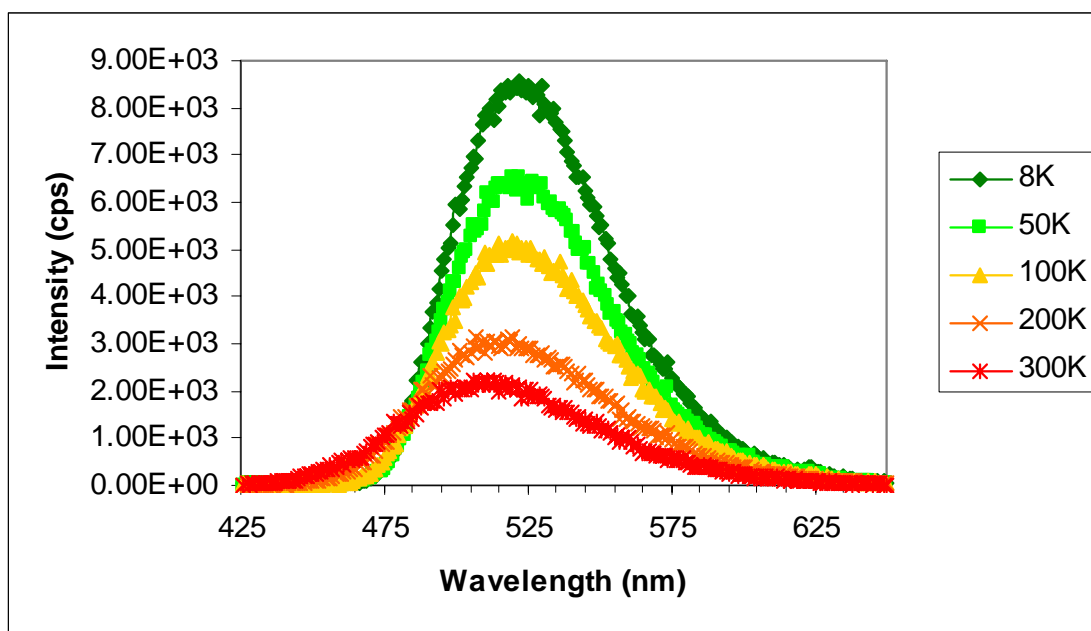


Figure 21 Low-temperature Luminescence Spectra of $Ba_2ZnSi_2O_7:Eu^{2+}$

6.3.3 $Ba_3ZnSi_2O_8:Eu^{2+}$

The low-temperature luminescent spectrum of $Ba_3ZnSi_2O_8:Eu^{2+}$ was measured, the sample was pumped using the same conditions discussed in section 6.3.1. The luminescence spectrum consisted of a broad peak at 535nm. A blue-shift of 35nm in the emission wavelength was observed as shown Figure 22.

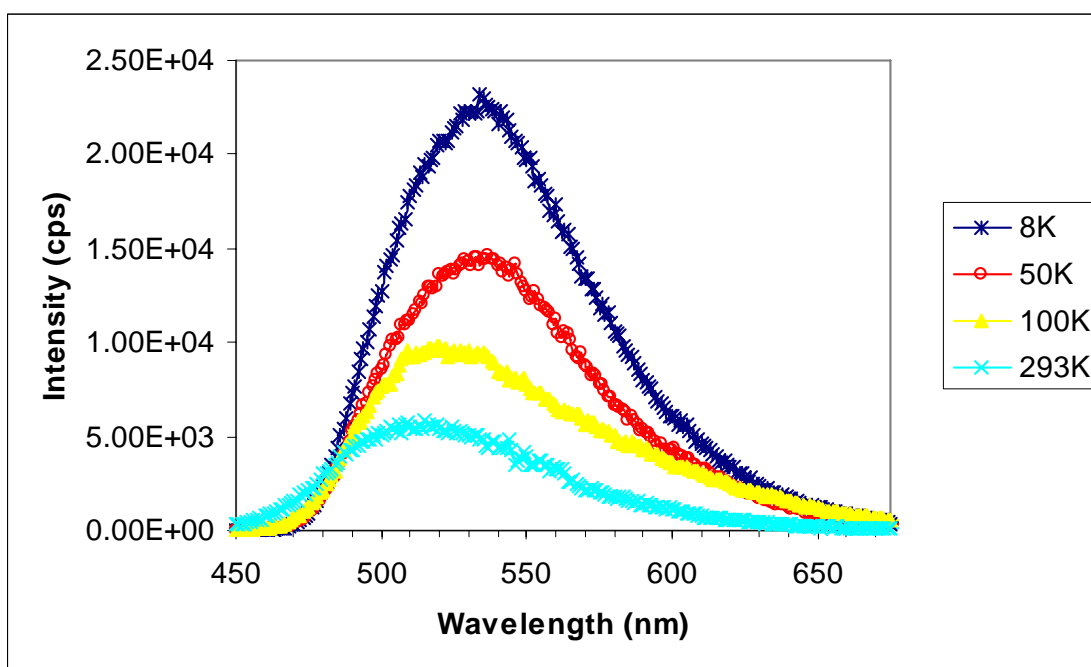


Figure 22 Low-temperature Luminescence Spectra of $Ba_3ZnSi_2O_8:Eu^{2+}$

6.4 Discussion

6.4.1 Energy Levels of Eu^{2+}

In general, site occupation is determined by ionic size. In the phosphor $Sr_2MgSi_2O_7$ and $Ba_2MgSi_2O_7$ or other strontium/barium silicates, Eu^{2+} (ionic radius of 1.09Å) will replace

Sr^{2+} (1.12Å) or Ba^{2+} (1.34Å), while Mn^{2+} (0.80Å) will substitute for Mg^{2+} (0.66Å) or Zn^{2+} (0.74Å). The Si^{4+} (0.42Å) is too small for Eu^{2+} or Mn^{2+} to substitute.

6.4.2 Eu^{2+} Energy Structure in the Crystal Lattice

Eu^{2+} has an electronic configuration $4f^7$. The $4f$ shell is just half filled. According to Hund's rule, the ground state of Eu^{2+} is ^8S . That is, the total orbital quantum number of the seven $4f$ electrons is $L=0$, and all spins are parallel with a total spin quantum number $S = \frac{7}{2}$.

The first excited state of Eu^{2+} ions is $^6\text{P}_{7/2}$ ($L=1$, $S=\frac{5}{2}$), 32000 cm^{-1} (310nm) above the ground state.

One of $4f$ electrons of Eu^{2+} can be relatively easy to excite to $5d$ shell to form a $4f^6 5d^1$ configuration, which is about 50000 cm^{-1} above the ground state ^8S . There are two states of $4f^6 5d^1$: high-spin state $4f^6 (\uparrow)5d^1(\uparrow)$ with spin degeneracy 8 manifolds; low-spin state $4f^6 (\uparrow)5d^1(\downarrow)$ with spin degeneracy 6 manifold. According to Hund's rule, the high spin state is lower in energy than the low spin state. The transition from high spin state to the ground state ^8S is both electronic dipole and spin allowed, and has a very high transition probability. The transition from low-spin state to the ground state is spin forbidden, and is used to be very weak.

In cubic lattice field, $5d^1$ state will split into E and T states. In the crystal lattice of low symmetry, the E and T states can be further split into two and three orbital singlets, respectively. E state stays at much higher energy, and can not be observed in UV ($\lambda >$

200nm). However, the T states can be lowered by the crystal field. They can be below ${}^6P_{7/2}$ of free ion Eu^{2+} and serve as metastable state. The UV bands shown in the excitation spectra of Sr and Ba silicates discussed previously are the absorption occur due to a transition from the ground state 8S to three field components of the T state. In most cases, three overlapped UV bands are observed. Sometimes, the splitting of T state is not large, or T splits into a doublet and a singlet and only one or two bands are resolved.

The remaining $4f$ electrons can couple with a $5d^1$ electron in the configuration $4f^6 5d^1$, and provide weak sharp lines over the $5d$ bands. But in most cases, the sharp lines are weak, and do not show up in the excitation spectrum.

6.4.3 Evaluation of the Silicate Phosphors

Under UV excitation, $\text{Sr}_2\text{MgSi}_2\text{O}_7:\text{Eu}^{2+}$, Mn^{2+} provides strong deep blue emission at 448nm and red-emission 656nm. If combined with the efficient green emission centered at 520nm of $\text{Ba}_2\text{ZnSi}_2\text{O}_7:\text{Eu}^{2+}$, Mn^{2+} or $\text{Ba}_3\text{ZnSi}_2\text{O}_8:\text{Eu}^{2+}$, Mn^{2+} , it is possible to develop white light sources of LED-tricolor phosphor.

Luminescence Center	Chemical Composition	Peak wavelength (nm)	Luminescence Color
Eu^{2+} , Mn^{2+}	$\text{Sr}_2\text{MgSi}_2\text{O}_7:\text{Eu}^{2+}$, Mn^{2+} (#1j)	(458), 672	Blue
Mn^{2+}	$\text{Ba}_3\text{ZnSi}_2\text{O}_8:\text{Mn}^{2+}$ (#33)	(378), 400	Blue
Eu^{2+} , Mn^{2+}	$\text{Ba}_3\text{ZnSi}_2\text{O}_8:\text{Eu}^{2+}$, Mn^{2+} (#39)	503	Green
Eu^{2+}	$\text{Sr}_2\text{ZnSi}_2\text{O}_7:\text{Eu}^{2+}$ (#34)	494	Green
Eu^{2+}	$\text{Ba}_2\text{ZnSi}_2\text{O}_7:\text{Eu}^{2+}$ (#36)	504	Green
Eu^{2+} , Mn^{2+}	$\text{Ba}_2\text{ZnSi}_2\text{O}_7:\text{Eu}^{2+}$, Mn^{2+} (#37)	554	Orange
Eu^{2+}	$\text{Ba}_3\text{ZnSi}_2\text{O}_8:\text{Eu}^{2+}$ (#38)	505	Green
Eu^{2+} , Mn^{2+}	$\text{Ba}_2\text{MgSi}_2\text{O}_7:\text{Eu}^{2+}$, Mn^{2+} (#40)	512	Green

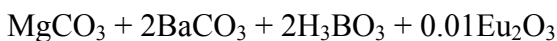
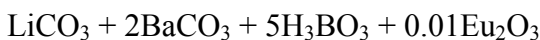
Table 3 Results for the Silicates

7 SPECTROSCOPY OF BORATES

It was previously reported in the literature (Dirksen & Blasse 1991) that $\text{LiBa}_2\text{B}_5\text{O}_{10}:\text{Eu}^{2+}$ showed a strong red emission band at 630nm. This emission has an unusual large Stoke shift ($\sim 11,000 \text{ cm}^{-1}$) and a moderate thermal quenching. The large Stoke shift was attributed to an off-center displacement of the Eu^{2+} ion at the irregular and large Ba^{2+} site. This work stimulated us to investigate borate phosphors.

7.1 Sample Preparation Details

Two borates were prepared: $\text{LiBa}_2\text{B}_5\text{O}_{10}:\text{Eu}^{2+}$ and $\text{Ba}_2\text{MgB}_2\text{O}_6:\text{Eu}^{2+}$. The samples were prepared according to the following recipes:



According to Dirksen and Blasse, no counter parts of $\text{LiBa}_2\text{B}_5\text{O}_{10}$ for Mg, Ca and Ba existed. In the recipes, B_2O_3 from the composition of H_2BO_3 is one of the principal ingredients. No additional flux is needed. The compounds are expected to have lower melting temperature. After grinding and pellet-pressing the $\text{LiBa}_2\text{B}_5\text{O}_{10}$ and $\text{Ba}_2\text{MgB}_2\text{O}_6$ sample were pre-fired at 500°C and 650°C , respectively. After the second grinding and pellet-pressing, the samples were finally fired at 650°C and $1,000^\circ\text{C}$ in $\text{N}_2+5\%\text{H}_2$ flow for 3hrs and 1hr, respectively.

A special care has been given to the sample of $\text{LiBa}_2\text{B}_5\text{O}_{10}:\text{Eu}^{2+}$ in order to compare with the results from Dirksen and Blasse. Those samples were re-sintered for three times.

Each time before re-sintering, additional grinding was taken in order to have a chemical reaction of all the reactants.

7.2 Excitation and Luminescence Spectra of $\text{LiBa}_2\text{B}_5\text{O}_{10}:\text{Eu}^{2+}$

The excitation and luminescent spectra of $\text{LiBa}_2\text{B}_5\text{O}_{10}:\text{Eu}^{2+}$ are given in Figure 23. It is surprisingly to note that the emission band is located at 508nm, instead of 630nm, as reported by Dirksen and Blasse.

In order to identify the sources in the difference of the result, great effort has been made to improve the crystalline structure of the samples. X-ray diffraction was taken on the sample. The XRD pattern is shown in Figure 23. For comparison, reference data from Huang et al. 1986 is reproduced in Figure 23. It can be seen from Figures 23 and 24 that our sample shows the same XRD pattern, and therefore has same crystal structure as reported in literature.

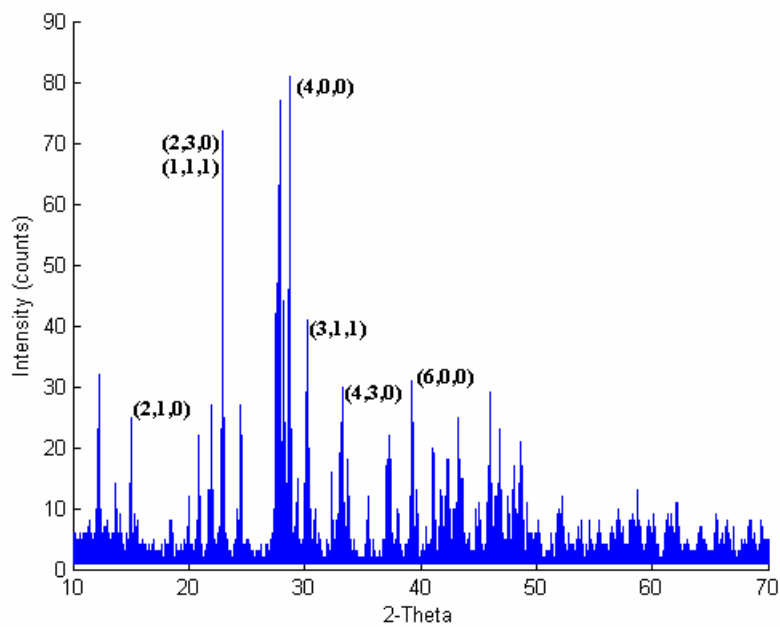


Figure 23 XRD Pattern for $\text{LiBa}_2\text{B}_5\text{O}_{10}:\text{Eu}^{2+}$

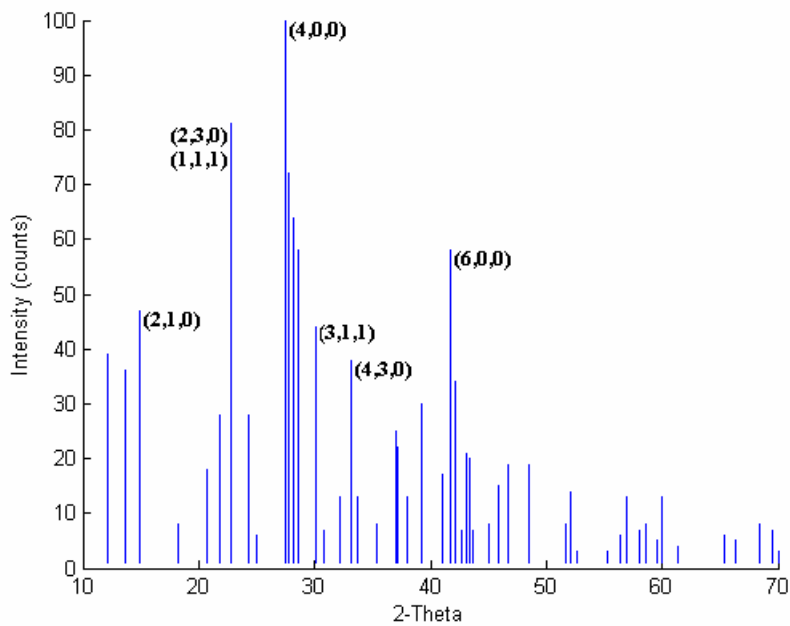


Figure 24 XRD Pattern for $\text{LiBa}_2\text{B}_5\text{O}_{10}$ (Huang et al. 1986)

Luminescence Center	Chemical Composition	Peak wavelength (nm)	Luminescence Color
Eu ²⁺	LiBa ₂ B ₅ O ₁₀ : Eu ²⁺ (#15)	508	Blue-green
	LiCa ₂ B ₅ O ₁₀ : Eu ²⁺ (#17)	611	Orange
	Ba ₂ MgB ₂ O ₆ : Eu ²⁺ (#31)	600	Orange

Table 4 Results for the Borates

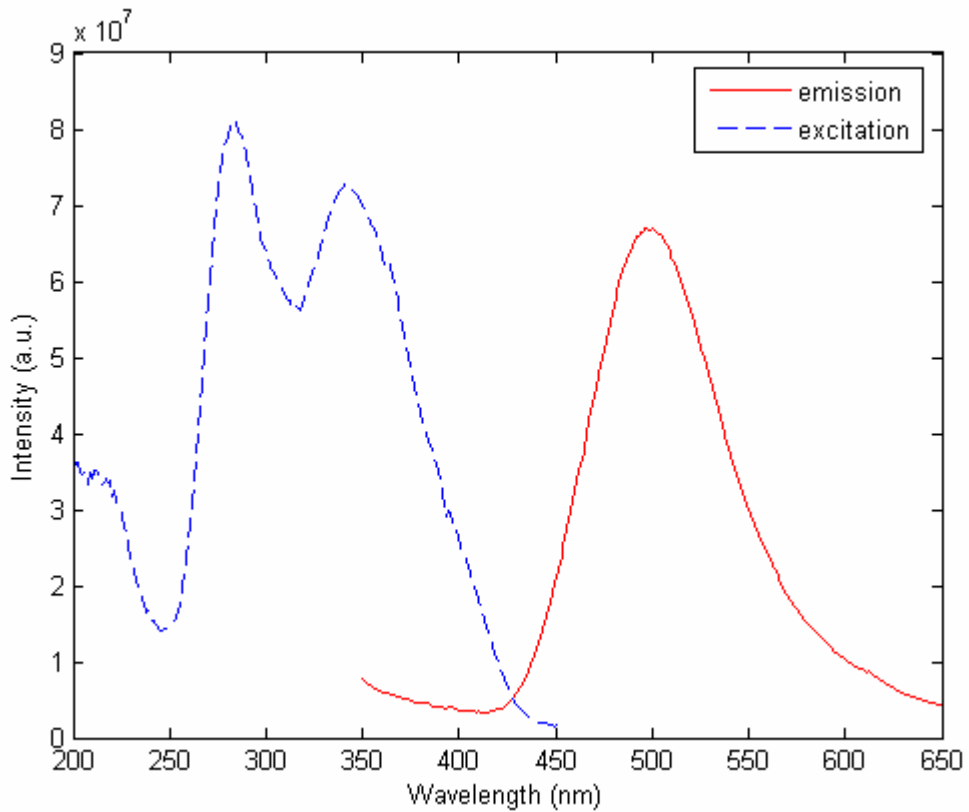


Figure 25 Luminescence ($\lambda_{ex} = 341\text{nm}$) and Excitation ($\lambda_{em} = 498\text{nm}$) Spectrum of LiBa₂B₅O₁₀:Eu²⁺

$\text{LiBa}_2\text{B}_5\text{O}_{10}$ has an orthorhombic structure with unit cell constants $a = 13,033$, $b = 14,360$ and $c = 4,246 \text{ \AA}$. The structure of this pentaborate contains one dimensional chain of polyborate anions built from BO_3 and BO_4 groups as shown in figure 26.

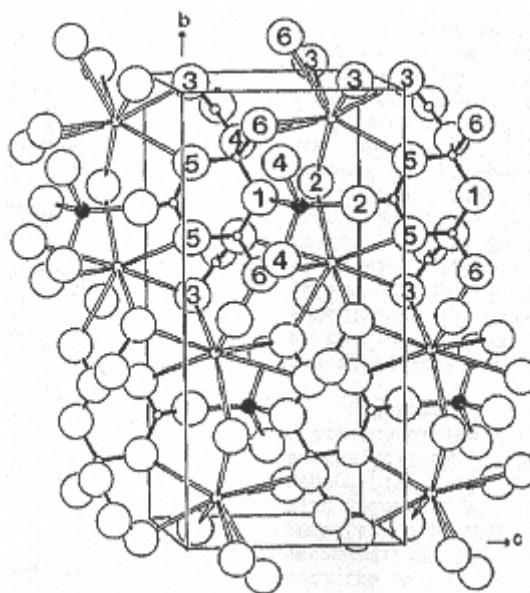


Figure 26 Drawing of the structure of $\text{LiBa}_2\text{B}_5\text{O}_{10}$. The largest open circles represent O atoms and the filled circles represent Li atoms. B-O interactions are designated by shaded bonds. The numbers in circles are used to label oxygen ions at different sites. (Smith and Keszker 1989)

The chains in the compound are interconnected by Li atoms in a distorted tetrahedral site and a Ba atom located in an irregular eight-coordinate site, as shown in the previous figure. The vertices of the Li-centered tetrahedron derive from three O_1 and 2O_4 on one chain and the apex atom O_2 of the bridging BO_3 group on another chain. The anion is comprised of two crystallographically independent trigonal BO_3 groups approximately centered by B_1 and B_2 and one distinct tetrahedral BO_4 group (Smith and Keszler 1989). From the crystal structure, there is only one type of Ba sites, and therefore, only one site of Eu^{2+} emission can

be observed. This argument excludes the possibility that the wavelength difference of the emission bands is related with different site occupation of Eu^{2+} . This is still an open question we can not answer at current stage.

7.3 Excitation and Luminescence Spectra of $\text{Ba}_2\text{MgB}_2\text{O}_6:\text{Eu}^{2+}$

The XRD pattern of $\text{Ba}_2\text{MgB}_2\text{O}_6:\text{Eu}^{2+}$ is shown in Figure 27. The pattern indicates that the sample has a good crystallinity.

This sample shows a very strong emission in the orange part of the spectrum at a wavelength of 600nm. The excitation spectrum shows a shoulder at 375nm and double peaks at 265 and 310nm. This structure is certainly related with the split T state of $5d$ levels. The strong orange emission makes the phosphor very attractive as a red component for LED-tricolor phosphor devices.

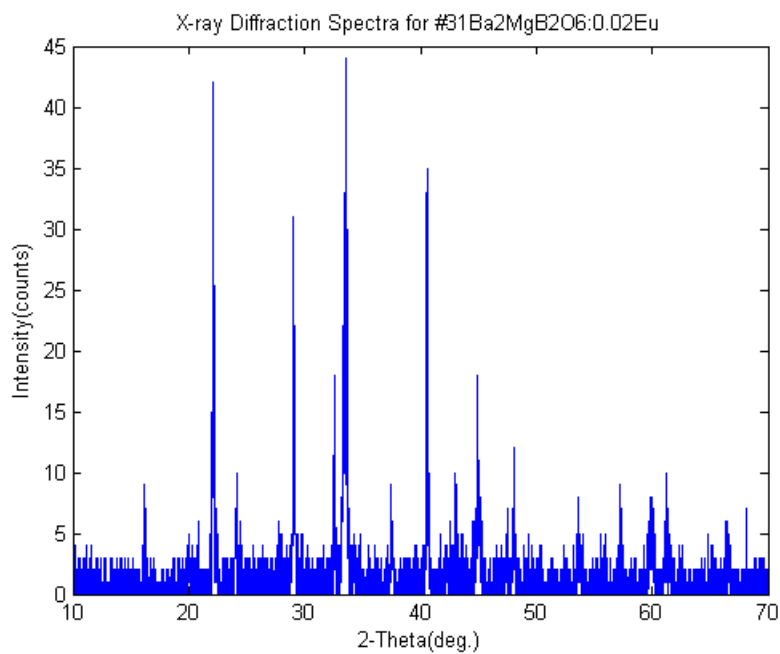


Figure 27 XRD Pattern for $\text{Ba}_2\text{MgB}_2\text{O}_6:\text{Eu}^{2+}$

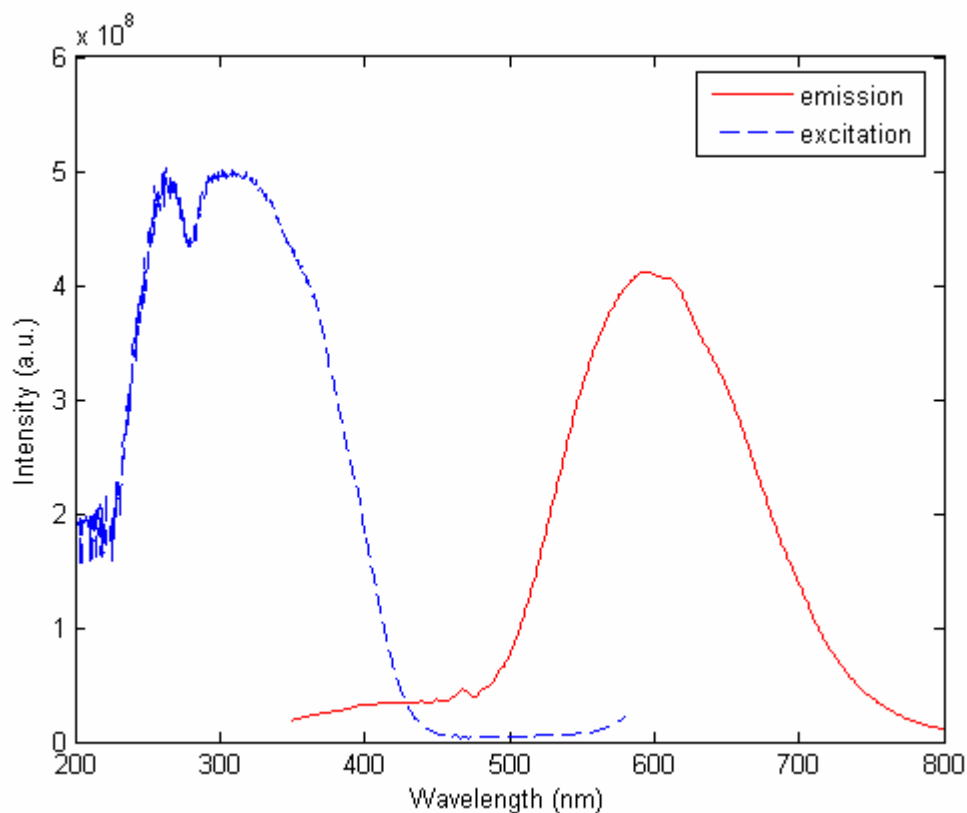


Figure 28 Luminescence ($\lambda_{ex} = 275\text{nm}$) and Excitation ($\lambda_{em} = 598\text{nm}$) Spectrum of $\text{Ba}_2\text{MgB}_2\text{O}_6:\text{Eu}^{2+}$

7.4 Low-Temperature Luminescence Spectra

7.4.1 $\text{LiBa}_2\text{B}_5\text{O}_{10}:\text{Eu}^{2+}$

The low-temperature luminescent spectrum of $\text{LiBa}_2\text{B}_5\text{O}_{10}:\text{Eu}^{2+}$ was measured with a SPEX double spectrometer 1403. The sample was pumped using the 351nm emission line of an Ar laser. The luminescence spectrum consists of two parts as shown in Figure 29. The UV part consists of three sharp lines at 368.5, 369.5 and 375.0nm. The detailed spectrum is shown in Figure 31.

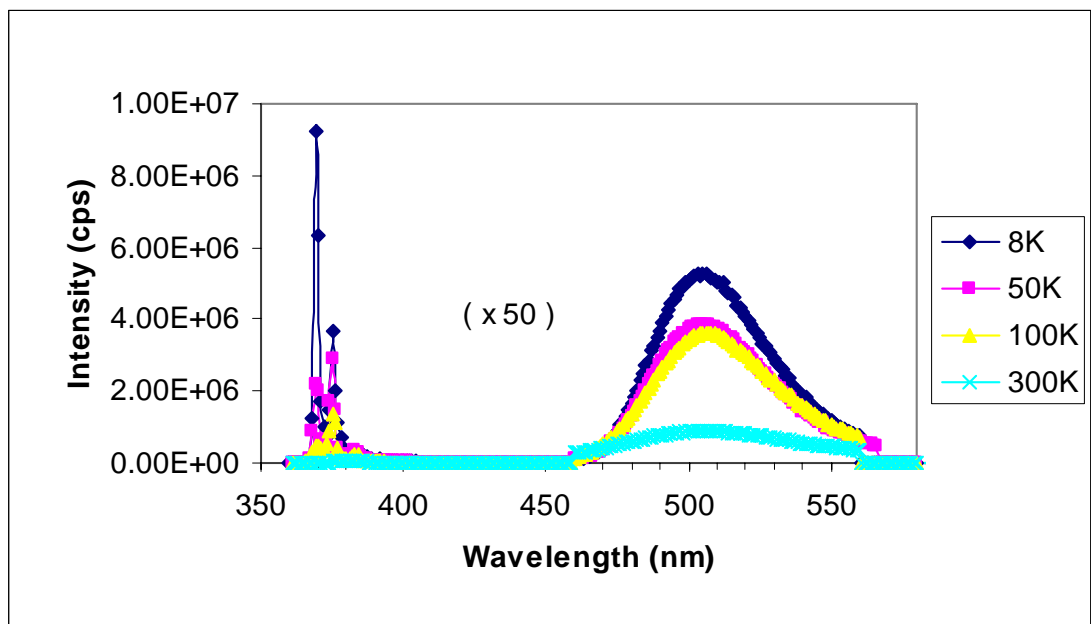


Figure 29 Low-temperature Luminescence spectra of $\text{LiBa}_2\text{B}_5\text{O}_{10}:\text{Eu}^{2+}$

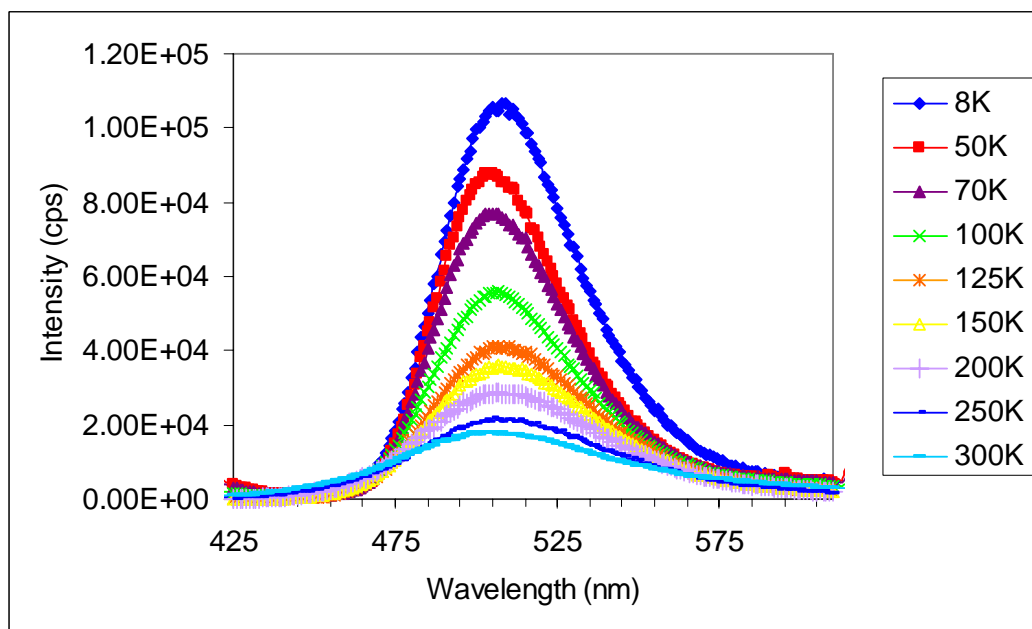


Figure 30 Low-temperature Luminescence Spectra of $\text{LiBa}_2\text{B}_5\text{O}_{10}:\text{Eu}^{2+}$

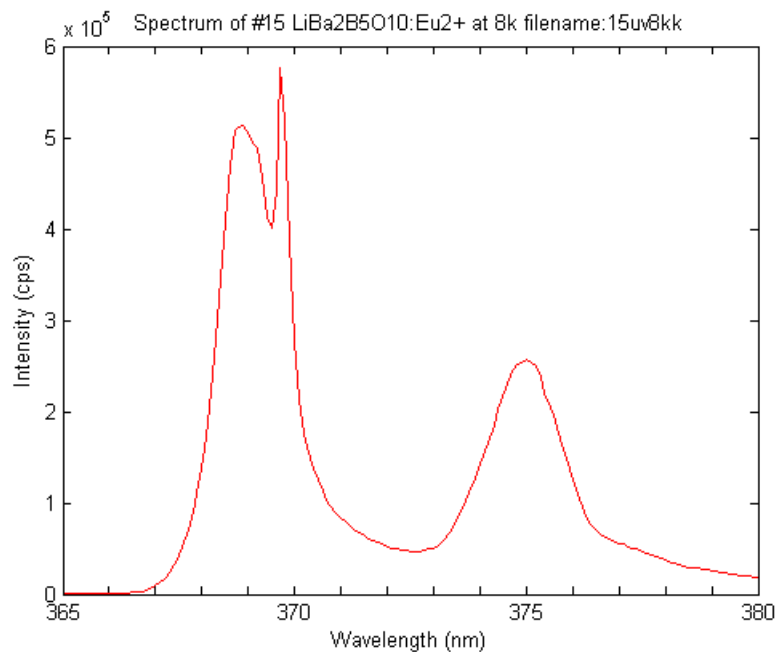


Figure 31 High-resolution Luminescence Spectrum of LiBa₂B₅O₁₀:Eu²⁺ measured at a temperature of 8K

The visible part is a broadband peaking at 508nm. Figure 30 shows the dependence of the emission band on temperatures. With increasing temperature, the band slightly shifts to the blue from 508nm(8K) to 504nm(300K)m and the intensity decreases. It is obvious that the green emission band at 508nm is originated from Eu²⁺. The UV emission is certainly not related with the doping ion. It must be from defect centers or deep bound excitons.

7.4.2 Undoped LiBa₂B₅O₁₀

In order to identify the source of the UV emission, undoped LiBa₂B₅O₁₀ was prepared. The sample was sintered in air. The intense UV emission spectrum, similar to that of LiBa₂B₅O₁₀:Eu²⁺ was also observed (Figure 32). In other words, the UV emission is indeed from the host. It is assumed to be from deep bound excitons, which are related with some

defects. In addition, it should be noted that the existence of the UV emission does not depend on the sintering condition, in reducing or oxidizing atmosphere, and also does not depend on if a foreign impurity ion is substituted.

It should be mentioned that a crystal host, which show efficient exciton emission, must be a good “semiconductor”. ZnO, AlN, GaN, ZnS, etc. are examples. We hope that $\text{LiBa}_2\text{B}_5\text{O}_{10}$ holds these promising characteristics.

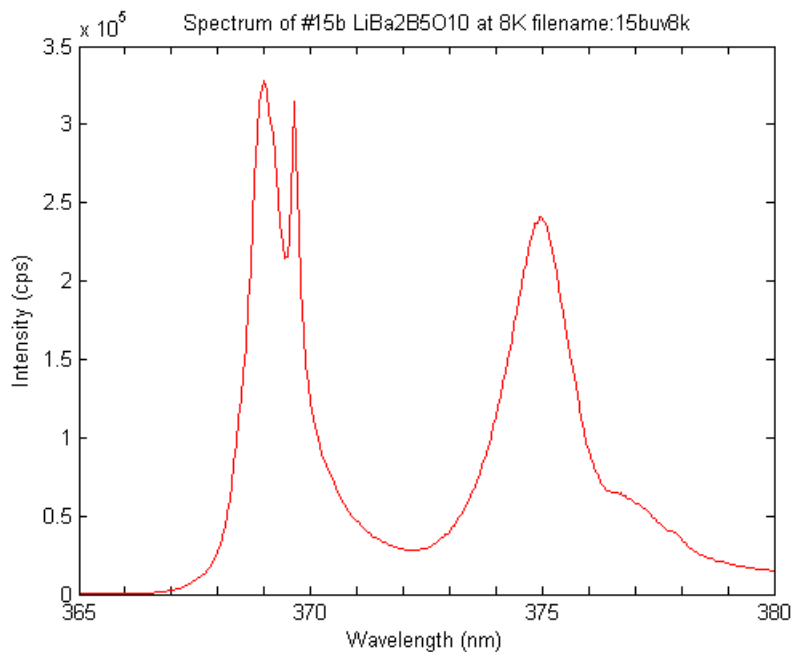


Figure 32 High-resolution Luminescence Spectrum of $\text{LiBa}_2\text{B}_5\text{O}_{10}$ measured at a temperature of 8K

7.4.3 $Ba_2MgB_2O_6:0.02Eu^{2+}$

Temperature dependence of luminescence of $Ba_2MgB_2O_6:Eu^{2+}$ was also measured. The results are given in Figure 33. With increasing temperature, the emission band shifts to the blue from 625nm(8K) to 595nm(300K), and the luminescence intensity decreases rapidly. It should be pointed out, that the peak position of the emission band at room temperature appeared to shift to 620nm in contrast to the value 600nm measured by the Fluoromax 2. That is because, unlike the Fluoromax 2, the SPEX 1403 we used is not spectral-calibrated. This shift is not real.

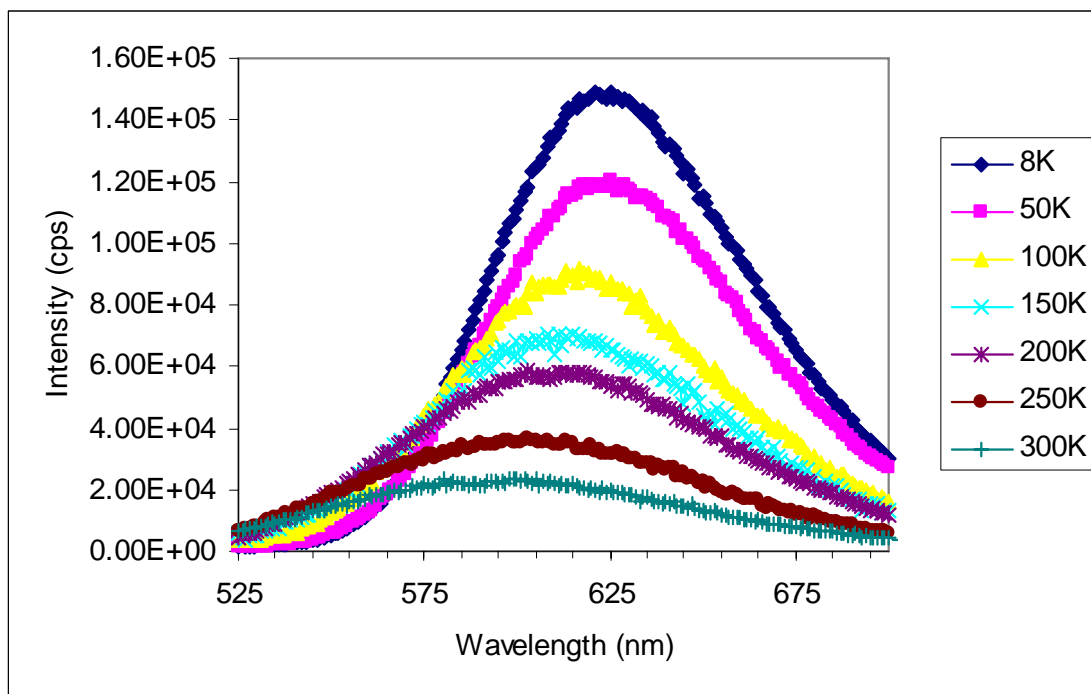


Figure 33 Low-temperature Luminescence Spectra of $Ba_2MgB_2O_6:Eu^{2+}$

7.5 Discussion: Blue-shift of Emission Bands

In section 6.3 and 7.4 we measured the dependence of emission bands from Eu^{2+} and Mn^{2+} . It was found that (1) the intensity emission decreases with increasing temperature; (2) the emission band was shifted to the red for Mn^{2+} , but shifted to the blue for Eu^{2+} . In section 2.5, we introduced the Single Configuration Coordinate (SCC) model. It can be used to explain the red-shift of emission and thermal quenching of luminescence. A photon with an energy E can excite an electron from the ground state to the excited state (process 1). At lower temperature, the electron returns to the ground state through process 2 and emits a photon with a small energy E_2 . At higher temperature, the electron thermally populates upper vibronic levels (process 3), and returns to the ground state and emits a photon with an even smaller energy E_4 ($E_4 < E_2$). This means, that a red-shift is observed.

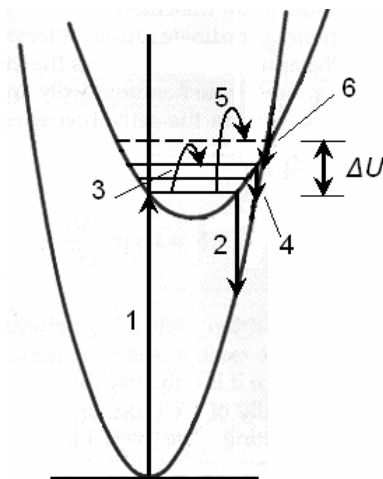


Figure 34 SCC Model for $3d$ Ions

At a much higher temperature, electrons have the probability to be activated over the energy barrier ΔU , and non-radiative returns to the ground state occur. The higher is the

temperature the more electrons return to the ground state non-radiatively. This causes a decrease of the luminescence. However, this model can not be used to explain the blue-shift of Eu^{2+} emission. A new modified SCC model is presented.

As we mentioned before, all $4f$ electrons are shielded from the crystal environment. In other words, interactions between $4f$ electrons and the lattice are negligible. The energy level for $4f$ states is:

$$U = \frac{1}{2}kQ^2 + E_0 \approx E_0.$$

As a result, straight horizontal lines are used to describe the energy levels of $4f$ electrons. Transitions between $4f$ levels are sharp lines and have no Stoke shift and no obvious spectral shift with increasing temperature. These are consistent with the experimental observations.

For the case of Eu^{2+} , all the electrons stay in $4f$ orbits at the ground state, and the energy curve should be a horizontal straight line. However, for the $4f^6 5d^1$ state, $5d$ electrons strongly couples with ligands, and the effective energy should be described by a potential curve. The modified Single Configuration Coordinate model is shown in the next Figure.

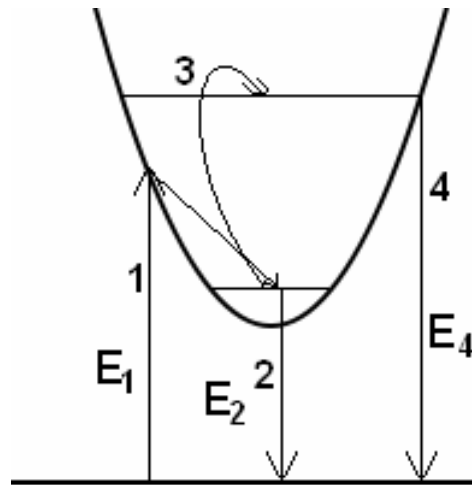


Figure 35 Schematic of the Blue-shift theory Energy Levels

After photon excitation, the electron emits photon with energy E_2 at low-temperature. At higher temperature, the higher vibronic states can be populated and the emitted photons may have larger energy (E_4). Then a blue-shift should be observed. The red-shift depends on thermal population of high vibronic energy levels and also depends on the strength of electron-phonon coupling. Stronger coupling corresponds to a larger force constant K (a steeper potential curve). Different host provide different lattice environment and geometry to give different electron-phonon coupling of doping ions. A challenge question still remains. The new single configuration coordinate model can not be used to explain the thermal quenching of luminescence, that is, decreasing of luminescence intensity observed in all Eu^{2+} doped phosphors. Then we need to seek other mechanism for the phenomenon.

As we mentioned on section 2.4, photo-excitation can be transferred to quenching centers, which could be lattice defects or un-intentional impurities. Such luminescence killer always exists to more or less extent in phosphors. Energy transfer from emission ions to

quenching centers can be thermally activated, and lead to decreasing of luminescence intensity.

8 CONCLUSIONS AND FUTURE WORK

$\text{Mg}_2\text{P}_2\text{O}_7:\text{Eu}^{2+}$, Mn^{2+} and $\text{Sr}_2\text{MgSi}_2\text{O}_7:\text{Eu}^{2+}$, Mn^{2+} are very promising phosphors, having two basic colors (blue and red), for LED-phosphor white light sources. These phosphors can be used in combination with the efficient green emission of some samples that we studied like $\text{Ba}_2\text{ZnSi}_2\text{O}_7:\text{Eu}^{2+}$, Mn^{2+} , $\text{Ba}_3\text{ZnSi}_2\text{O}_8:\text{Eu}^{2+}$, Mn^{2+} , $\text{Ba}_3\text{ZnSi}_2\text{O}_8:\text{Eu}^{2+}$, $\text{Sr}_2\text{ZnSi}_2\text{O}_7:\text{Eu}^{2+}$ and $\text{Ba}_2\text{ZnSi}_2\text{O}_7:\text{Eu}^{2+}$. $\text{LiBa}_2\text{B}_5\text{O}_{10}:\text{Eu}^{2+}$ and $\text{Ba}_2\text{MgB}_2\text{O}_6:\text{Eu}^{2+}$ are also very interesting materials for LED-phosphor applications. $\text{LiBa}_2\text{B}_5\text{O}_{10}:\text{Eu}^{2+}$ might be an interesting wideband gap semiconductor. In this case more work needs to be done, for example, to measure the exciton absorption and emission temperature dependence.

We propose a modified single coordinate configuration model in order to explain the blue-shift of Eu^{2+} emission with increasing temperature. In order to further confirm this new model, more work needs to be done. For example, low-temperature excitation spectra need to be measured to reveal how the $5d$ level (absorption) depends on temperature. Then the net contribution from phonon-electron interaction can be obtained.

9 REFERENCES

1. [Anonymous]. 2006. Light-Emitting Diodes. Schematic of a Light-Emitting Diode. <http://tellus.ssec.wisc.edu/outreach/gifts/sp_measure/page2.htm>.
2. Akella, A. and Keszler, D.A. 1995. Mat Res Bull. 30(1)105-111.
3. Ashcroft, N.W. and Mermin, N.D. 1976. Solid State Physics. Hecourt, Inc. pp308-309.
4. Ballato, J., Lewis III, J. S. and Holloway. 1991. MRS Bulletin. Sept (1991) 51.
5. Batler, K. H. and Jerome, C.W. 1950. J Electrochem Soc. 97. 265pp.
6. Blasse, G. 1973. Phys Stat Sol. 55. K131pp.
7. Blasse, G. and Brabmairer, B. C. 1994. Luminescence Materials. Springerverlag, New York. p108.
8. Dieke, G.H. 1968. **Spectra and Energy Levels of Rare Earth Ions in Crystals**. Wiley Interscience, New York.
9. Dirksen, G.J. & Blasse, G. 1991. J Sol State Chem. 92. 591-593.
10. Ferrari M., Campostrini R., Carturan G. and Montanga M. 1992. **Spectroscopy of trivalent europium in gel-derived silica glasses**. Philos Mag Phys Condes Matter Electron Opt Magn Prop. 65(2):251-260.
11. Goldberg, P. 1966. **Luminescence of Inorganic Solids**. Academy Press Inc., New York, USA. pp765.

12. Henderson, B. and Imbusch, G. F. 1989. **Optical Spectroscopy of Inorganic Solids**. Oxford University Press, NY, USA. 645pp.
13. Huang, Q., Wang, G. & Liang, J. 1984. Acta Phys Sinica. Wuli Xuebao. 33 p76.
14. Jia, D., Jia, W., Evans D. R., Dennis, W.M., Liu, H., Zhu, J. and Yen, W.M. 2000. J App Phys. 88(6). 3402-3407.
15. Jia, W., Jia, D., Rodríguez, T., Evans, D.R., Meltzer, R.S. and Yen, W.M. 2006. J Lumin. 119-120. 13-18pp.
16. Jia, W., Yuan, H., Holmstrom, S., Liu, H. and Yen, W.M. 1999. J Lumin. 83-84. 465-469pp.
17. Jia, W., Yuan, H., Lu, L., Huimin, L. and Yen, W.M. 1998. J Crys Gro. 200. 179-184pp.
18. King, C. N. 1996. J SID. 4/3 153.
19. Kojima, T. 1999. **Phosphor Handbook**. CRC Press, Boca Ratón.
20. Lehman, W. 1978. **Phosphor Cookbook**. Westing House, R & D Center. p116.
21. Leskelä, M. 1998. J Alloys Comp. 702:275-277.
22. MacDonagh, C., O'Kelly, B.O., Delvin, K., Tang, Z. R. and McGilp, J. M. 1990. **Optical Characterization of sol-gel Glasses: New Materials and their Applications**. Proceedings of the 2nd international Symposium. Warwick, UK. 10-12 April. pp435-440.
23. McClure, D.S. and Pedrini, C. 1985. Phys Rev B. 32 8465.
24. Morimoto, K. 1999. Phosphor Handbook. CRC Press, Boca Ratón.

25. Nakazawa, E. and Shionoya, S. 1970. J Phys Soc Japan. 28(1260).
26. Poort, S.H.M. and Blasse, G. 1997. J Lumin. 72 - 74. 247-249.
27. Rivera-Figueroa, I. 2001. [M.S. Thesis] **Photoluminescence of Pr³⁺ Doped CaTiO₃ Phosphor**. University of Puerto Rico Mayagüez. Available from University of Puerto Rico Mayagüez Campus Library.
28. Rubio O., J. 1991. J Phys Chem Solids. 52 (1). pp101-174.
29. Shionoya, S. and Yem, M.W. 1999. **Phosphor Handbook**. CRC Press LLC, Boca Raton Florida, USA.
30. Smith, R. W. and Keszler, D. A. 1989. Mat Res Bull. 24:725-731.
31. Sobel, A. 1998. Sci Am. 70 278.
32. Van Uitert, L.G. 1960. **Factors Influencing the Luminescent Emission States of Rare Earths**. J Elec Soc. 107:803.
33. Van Uitert, L.G. 1966. Luminescence of insulating solids for optical masers. Academic Press, New York, USA. pp 778.
34. Walterelt, P., Brandt, O., Trampert, A., Grahn, H. T., Menniger, J., Ramsteiner, M., Reiche, M. and Ploog, K. H. 2000. Nature. (406) 865.
35. Wargin, W. and Karapetyan. 1959. Absorption spectra and luminescence of glasses containing Ce. Glastechn. Ber. 32(11):443-450.
36. Weller, T. 1991. J Lumin. 48 & 49. 49p.
37. Zhu, C., Chen, X., Yuan, S., Yang, Y. and Chen, G. 2005. Photoluminescence and γ -ray irradiation of SrO-B₂O₃-P₂O₅:Eu²⁺ and SrMoO₄:Eu³⁺ phosphors. Institute of Inorganic Materials, Shanghai & CR ENEA CASACCIA Rome, Italy.
38. Zukauskas A., Shur M. S. and Gaska R. MRS Bulletin. 26 (2001) 764.

APPENDIX A

TABLE OF THE SAMPLES PREPARED

Sample	Chemical Composition	Pre-Sintering Temp. & time (°C)	Sintering Temp. & time (°C) [N ₂ + 5% H ₂]	Color of Emission	Wavelength (nm)	Special Notes
#1	Sr ₂ MgSi ₂ O ₇ : 0.02 Mn	800, 3hrs	1300, 3hrs	None	-	Whitish grey
#2	Sr ₃ MgSi ₂ O ₈ : 0.02 Mn	800, 3hrs	1300, 3hrs	None	-	Dark grey
#3	Sr ₂ ZnSi ₂ O ₇ : 0.02 Mn	800, 3hrs	1300, 3hrs	None	-	Grey
#4	Sr ₃ ZnSi ₂ O ₈ : 0.02 Mn	800, 3hrs	1300, 3hrs	None	-	Black
#5	Sr ₂ P ₂ O ₇ :0.02 Mn	600, 2hrs	1200, 2hrs	Weak White		
#6	Ca ₂ P ₂ O ₇ :0.02 Mn	600, 2hrs	1200, 2hrs	None	-	Formed a paste during mortaring
#7	Ba ₂ P ₂ O ₇ :0.02 Mn	600, 2hrs	1200, 2hrs	None	-	
#8	Mg ₂ P ₂ O ₇ :0.02 Mn	600, 2hrs	1200, 2hrs	Weak red	520, (690)	
#9	Sr ₃ (PO ₄) ₂ :0.02 Mn	600, 2hrs	1200, 2hrs	None	-	
#15*	LiBa ₂ B ₅ O ₁₀ : Eu ²⁺	500, 2hrs	650, 3hrs	Strong blue	498	Burned at 850°C
#16	LiSr ₂ B ₅ O ₁₀ : Eu ²⁺	500, 2hrs	650, 3hrs	None	-	Burned at 850°C
#17	LiCa ₂ B ₅ O ₁₀ : Eu ²⁺	500, 2hrs	750, 3hrs	Weak orange	611	
#18	LiMg ₂ B ₅ O ₁₀ : Eu ²⁺	500, 2hrs	800, 3hrs	None	-	
#19	MgBa ₂ B ₂ O ₆ : Eu ²⁺	500, 2hrs	1000, 2hrs	Weak red		
#20	MgSr ₂ B ₂ O ₆ : Eu ²⁺	500, 2hrs	1000, 2hrs	Weak red		Melted at 1,100°C
#21	MgCa ₂ B ₂ O ₆ : Eu ²⁺	500, 2hrs	1000, 2hrs	Red		Melted at 1,100°C
#22	Ca ₂ P ₂ O ₇ :0.02 Mn	600, 1hr	1250, 1hr	None	-	
#23	Ba ₂ P ₂ O ₇ :0.02 Mn	600, 1hr	1250, 1hr	None	-	
#24	Mg ₂ P ₂ O ₇ :0.02 Mn	600, 1hr	1100, 1hr	Weak red	675	
#25	Sr ₂ P ₂ O ₇ :0.02 Mn	600, 1hr	1250, 1hr	None	-	
#26*	Ca ₂ P ₂ O ₇ :0.02Eu,0.04 Mn	600, 1hr	1100, 1hr	Weak red	(422), 562	
#27	Ba ₂ P ₂ O ₇ :0.02 Eu, 0.04 Mn	600, 1hr	1100, 1hr	None	-	

#28*	Mg ₂ P ₂ O ₇ :0.02 Eu, 0.04 Mn	600, 1hr	1100, 1hr	Weak orange	(448), 656	
#29*	Sr ₂ P ₂ O ₇ :0.02 Eu, 0.04 Mn	600, 1hr	1100, 1hr	Strong blue	392, (420), 560	
#30	Ca ₂ P ₂ O ₇ : 0.02Eu, 0.06Mn	600, 1hr	1100, 1hr	None	-	
#31 *	Ba ₂ MgB ₂ O ₆ : 0.02Eu	650, 2hrs	1000, 4hrs	Strong Orange	600	
#32	Ba ₂ ZnSi ₂ O ₇ :8%Mn ²⁺	900, 3hrs	1200, 4hrs	None	-	
#33	Ba ₃ ZnSi ₂ O ₈ :8%Mn ²⁺	900, 3hrs	1200, 4hrs	Weak Blue	(378), 400	Intense green spots
#1j	Sr ₂ MgSi ₂ O ₇ :4%Eu ²⁺ , 8%Mn ²⁺			Green	(458), 672	
#34	Sr ₂ ZnSi ₂ O ₇ :0.01Eu ²⁺		1220, 4hrs	Weak Green	494	
#35	Sr ₃ ZnSi ₂ O ₈ :0.01Eu ²⁺			None	-	
#36	Ba ₂ ZnSi ₂ O ₇ :0.01 Eu ²⁺		1220, 4hrs	Strong Green	504	
#37	Ba ₂ ZnSi ₂ O ₇ :4%Eu ²⁺ , 8%Mn ²⁺		1180, 3hrs	Orange	554	
#38	Ba ₃ ZnSi ₂ O ₈ :0.01 Eu ²⁺		1220, 4hrs	Strong Green	505	
#39	Ba ₃ ZnSi ₂ O ₈ :4%Eu ²⁺ , 8%Mn ²⁺		1180, 3hrs	Strong Green	503	
#40	Ba ₂ MgSi ₂ O ₇ :4%Eu ²⁺ , 8%Mn ²⁺			Strong Green	512	

Table 5 Results for all the samples prepared during this research

* X-ray Diffraction profile available